

Boron-doped diamond nano/microelectrodes for biosensing and *in vitro* measurements

Hua Dong¹, Shihua Wang², James J. Galligan³, Greg M. Swain⁴

¹Department of Entomology and Cancer Research Center, University of California, Davis, CA, 95616, ²Department of Chemistry and Biochemistry, The University of Arizona, Tucson, AZ 85721, ³Department of Pharmacology and Toxicology, Michigan State University, MI 48824, ⁴Department of Chemistry, Michigan State University, MI 48824

TABLE OF CONTENTS

1. Abstract
2. Introduction
3. Deposition of boron-doped diamond (BDD) materials
 - 3.1. Synthetic diamond
 - 3.2. Deposition of nanocrystalline diamond
 - 3.3. Preparation of BDD Microelectrode
4. Characterization of BDD thin films
 - 4.1. Scanning electron microscopy
 - 4.2. Conductive probe atomic force microscopy
 - 4.3. Raman Spectra
 - 4.4. Electrochemical characterization
5. Application of BDD electrode for bio-sensing and *in vitro* measurement of biomolecules
 - 5.1. Continuous amperometry
 - 5.1.1. Norepinephrine measurement from rat mesenteric artery
 - 5.1.2. Serotonin (5-HT) measurement from guinea pig and rabbit intestinal mucosal layer, and rhesus monkey lymphocytes
 - 5.1.3. Nitric oxide measurement from guinea pig ileum
 - 5.1.4. Histamine measurement from oxyntic glands of guinea pig stomach
 - 5.2. Fast scan cyclic voltammetry
 - 5.2.1. Adenosine measurement from prebötzing complex in rat brain stem
 - 5.2.2. Serotonin (5-HT) measurement from *aplysia californica* metacerebral cell
6. Conclusions and perspective
7. References

1. ABSTRACT

Since the fabrication of the first diamond electrode in the mid 1980s, rapid progress has been made on the development and application of this new type of electrode material. Boron-doped diamond (BDD) electrodes exhibit outstanding properties compared to oxygen-containing sp^2 carbon electrodes. These properties make BDD electrodes an ideal choice for use in complex samples. In recent years, BDD microelectrodes have been applied to *in vitro* measurements of biological molecules in tissues and cells. This review will summarize recent progress in the development and applications of BDD electrodes in bio-sensing and *in vitro* measurements of biomolecules. In the first section, the methods for BDD diamond film deposition and BDD microelectrodes preparation are described. This is followed by a description and discussion of several approaches for characterization of the BDD electrode surface structure, morphology, and electrochemical activity. Further, application of BDD microelectrodes for use in the *in vitro* analysis of norepinephrine (NE), serotonin (5-HT), nitric oxide (NO), histamine, and adenosine from tissues are summarized and finally some of the remaining challenges are discussed.

2. INTRODUCTION

Traditional carbon electrode materials, such as glassy carbon, pyrolytic graphite and carbon fiber, are important for use in electrochemistry due to their low cost and simple preparation (1). However, these materials possess sp^2 -bonded carbon structure with an extended π -electron system and thus suffer from significant corrosion in the form of cavitations, pitting, and surface oxidation. Diamond has some unique properties such as high thermal conductivity, low coefficient of friction, chemical inertness, optical transparency between UV and IR wavelength, high mechanical stability, and high corrosion resistance (2). In 1983, the first report on the use of ion-implanted diamond as an electrochemical electrode marked the beginning of the era of diamond electrode (3). When doped with boron, diamond can be semi-conductive depending on the doping level and is suitable for use as an electrode (4, 5). There have been several reviews (6-9) over the past two decades that describe polycrystalline electrochemical, boron-doped diamond films, prepared by chemical vapor deposition (CVD) for electrochemistry. Due to the stable sp^3 bonded carbon structure without the extended π -electron system, BDD electrodes exhibit superior

performances compared to the traditional carbon electrode materials, including: (1) extremely wide potential window of water stability that enables the application of the anodic and cathodic potentials used for the detection of biological molecules; (2) lower background current which leads to improved signal to background and signal to noise ratio, and lower limit of detection; (3) good chemical and mechanical stability that lead to less molecular adsorption and resistance to fouling; (4) good electrochemical activity for redox systems without any pre-treatment and a fast response time (10-14). These characteristics make diamond thin film electrodes excellent electrochemical sensors to the analysis for various organic and inorganic species (9, 15, 16). Preliminary work of BDD electrodes as detectors of various bioanalytes, e.g., dopamine (17), norepinephrine (18), serotonin (19), nicotinamide adenine dinucleotide (NADH) (20), and sulfa drugs (21), have also shown the potential of diamond to be used as biosensors.

The first BDD microelectrode with steady state cyclic voltammogram was reported in 1998 (22). Only recently, have diamond microelectrodes been applied in the biological systems and shown to be very useful for the *in vitro* and *in vivo* measurements of electro-active neurosignaling molecules in complex biological systems (23-26). Although carbon fiber microelectrodes have long been used for *in vitro* measurement of biological molecules by amperometry and fast scan cyclic voltammetry (27-29), BDD microelectrodes have attracted numerous attentions because of its superb electrochemical properties that are mentioned above. BDD microelectrodes have a variety of geometries such as discal (30), cylindrical, spherical, hemispherical (31), conical (26), and beveled shape (32), with the diameters ranging from 5 to 100 μm . Among them, discal, cylindrical and conical shaped microelectrodes are most widely used for the *in vitro* neurotransmitter detection. These microelectrodes all have small tip dimension (less than 30 μm diameter), which provides a spatial resolution of 10-100 μm , to allow measurement within a limited space, such as a single cell, to be made. Compared to BDD macroelectrode, the small size of microelectrodes provide significantly higher spatial and temporal resolution, enhanced signal to noise ratio due to the small interfacial capacitance and lower background current, and minimum tissue damage (26, 33). For *in vitro* study, BDD microelectrodes can monitor the biological molecules from the recent release sites and provide information to study the release and clearance kinetics of these molecules.

This review focuses mainly on the fabrication and application of BDD electrode for *in vitro* bio-sensing and measurements of norepinephrine, serotonin, adenosine, histamine and nitric oxide. These neurotransmitters are widely distributed in mammalian species. Monitoring their levels in tissues or biological fluids, such as plasma, is of general importance (34-37). There are also other widely used methods to detect these neurotransmitters, including mechanical bioassay (38), and HPLC overflow techniques (18). However, these methods are in minute scale with poor temporal resolutions and the kinetics of neurotransmitter release cannot be measured. Through real-time detection with BDD microelectrodes, the time course of local

neurotransmitter release and clearance can be determined and the related mechanisms can be studied.

3. DEPOSITION OF BDD MATERIALS

3.1. Synthetic diamond

Natural diamond is an electrical insulator with a band-gap of ~ 5.5 eV and a resistivity greater than 10^{12} $\Omega\text{-cm}$ (39). However, the resistivity of synthetic diamond can be lowered to 10^6 $\Omega\text{-cm}$ when terminated with hydrogen (or having it incorporated into the lattice). In fact, diamond grown via chemical vapor deposition (CVD) in hydrogen-rich environments can exhibit the so-called "surface conductivity" (40). Synthetic diamond can be made more conductive via doping with elements such as boron, nitrogen and phosphorous. Diamond can be made p-type by doping with boron, $E_a = 0.37$ eV, and n-type by doping with nitrogen, $E_a = 1.7$ eV, or phosphorous, $E_a = 0.56$ eV (41). These are large activation energies compared to the activation energy for boron-doped Si (ca. 0.02 eV) (42). Boron is the most commonly used dopant (4, 5). Hydrogen can act as both a donor and an acceptor. Nitrogen is among a few suitable dopants for CVD diamond, but unfortunately it forms a deep donor level ~ 1.7 eV below the bottom of the conduction band. This is due to its structural distortion from the substitutional position in the diamond lattice. A breakthrough in synthesizing N-doped diamond came several years ago through the addition of N_2 to the CH_4/Ar source gas mixture for growing ultrananocrystalline diamond (43). Koizumi et al reported the growth of n-type diamond on (111)-oriented diamond substrates by using a mixture of PH_3 , CH_4 and H_2 gas in 1997 (44). Following this success, several studies have also been reported for phosphorous (P) doping during the chemical vapor deposition of diamond (41, 45, 46).

The most extensively employed synthetic diamond in electrochemistry is the p-type, boron-doped material. The resistivity of highly boron-doped diamond thin films can be as low as ~ 0.005 $\Omega\text{-cm}$. Both high-quality microcrystalline and nanocrystalline boron-doped diamond thin films can be routinely prepared now. However, low pressure diamond synthesis via CVD dates back to the 1950s and 60s when research was conducted in both the former Soviet Union and the United States (47, 48). Since then, developments in CVD technology have enabled the production of diamond for a number of applications, such as optical windows, wear-resistant coatings for cutting tools, thermistors, and electrodes (49). Several CVD growth methods exist for producing diamond, all of which utilize a carbon-containing reactant source gas (e.g., methane and hydrogen), an energy source to promote reactant dissociation (e.g., microwave, hot-filament, or DC discharge), and a substrate (e.g., Si, W, Mo). High-quality (i.e., low defect density and low nondiamond carbon impurity content) CVD diamond is typically produced at low pressure (10 to 500 Torr), high gas temperature (>1700 $^\circ\text{C}$), high substrate temperature (700 to 800 $^\circ\text{C}$), and low carbon concentration in the source gas (e.g., 0.5%) with an energy source for gas dissociation and radical formation (49, 50).

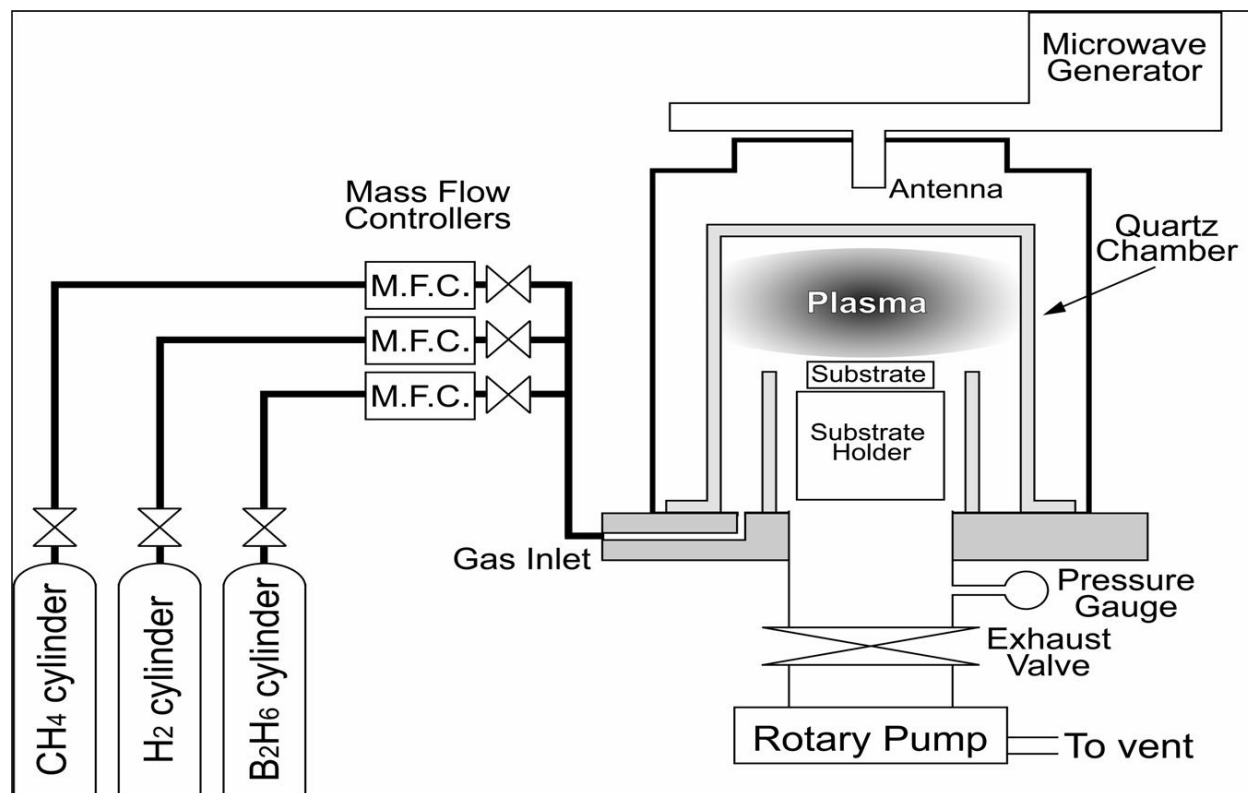


Figure 1. Schematic commercial MPCVD system (ASTex Inc., Lowell, MA) used for growing nanocrystalline boron-doped diamond thin films.

3.2. Deposition of nanocrystalline diamond

Diamond thin film can be deposited on several substrates (e.g. silicon, quartz, platinum, tungsten, molybdenum, titanium, tantalum, niobium and carbon) by either hot filament or microwave plasma-assisted CVD through well understood growth mechanisms (49, 51-53). Regardless of the type of substrate used, the surface of substrate must be seeded first, usually by being polished with diamond powder or ultrasonicated in a suspension of diamond nanoparticles (54). This is a prerequisite to enhance the initial nucleation density on nondiamond substrates. Coating with diamond-like carbon on the substrate is another possibility.

To date, there are two procedures for preparing nanocrystalline boron-doped diamond thin films. One procedure, developed by the Naval Research Laboratory group, involves the use of a conventional CH_4/H_2 source gas mixture, so-called nanocrystalline diamond (NCD) (55-57). Another method, developed by the Argonne National Laboratory group, involves the use of a $\text{CH}_4/\text{H}_2/\text{Ar}$ source gas mixture, so-called (ultra)nanocrystalline diamond (UNCD) (56, 58-61). CVD deposition of NCD from a H_2 -rich gas mixture is similar to that for conventional microcrystalline diamond (55-57). These films are faceted but the crystal size is small due to the short growth time and the high initial nucleation density that is achieved by proper substrate preparation and seeding. Films deposited from an Ar-rich mixture, on the other hand, are not faceted

but rather possess a nodular morphology with negligible crystal faceting (56, 58-61). Theoretical results suggest that the nanocrystalline morphology results, at least in part, from a high rate of renucleation due to C_2 dimer (59, 62-64). These UNCD films are very different from the NCD films as the former possess a smaller grain size, more grain boundaries, and sp^2 -bonded carbon atoms in these grain boundaries.

Figure 1 shows a typical schematic of microwave plasma-assisted chemical vapor deposition (MPCVD) system. The UNCD films are typically deposited using a 1% $\text{CH}_4/5\% \text{H}_2/94\% \text{Ar}$ source gas mixture for 2 h. The microwave power and system pressure are maintained at 800 W and 140 Torr, respectively. The substrate temperature is *ca.* 800 °C. Boron doping is accomplished by added B_2H_6 (from a 0.1% $\text{B}_2\text{H}_6/\text{H}_2$ gas mixture) to the source gas. The resulting film thickness is *ca.* 4 ~ 6 μm . The carrier concentration is in the low 10^{20}cm^{-3} range with a hole mobility between 0.1 and 1 $\text{cm}^2/\text{V s}$, as determined from Hall measurements. The film's electrical resistivity, as measured by a 4-point probe apparatus, is $\leq 0.01 \Omega\text{-cm}$ (65). On the other hand, a high-quality, hydrogen-terminated boron-doped NCD film is typically deposited in this way: the unseeded silicon wafer is placed in the microwave plasma reactor and exposed to the microwave plasma for 8 min at a system pressure of 15 Torr, a substrate temperature of 750 °C, and a microwave power of 800 W. A gas composition consisting of 900 sccm H_2 , 4 sccm of 0.1%

B₂H₆ in H₂, and 7 sccm CH₄ flowed through the chamber. The wafer is then removed and seeded with ultra-disperse nanodiamond particles in an ethanol suspension in an ultrasonic bath. The seeded wafer is returned to the chamber for growth (720 min) at a substrate temperature of 750 °C, a system pressure of 15 Torr, and a microwave power of 800 W. The gas composition flowing through the reactor is 900 sccm H₂, 4 sccm of 0.1% B₂H₆ in H₂, and 3 sccm CH₄. The resultant film is *ca.* 1.5 μm thick. The film has an in-plane resistivity near 0.01 Ω-cm, similar to the UNCD films (55, 57).

3.3. Preparation of BDD microelectrode

Diamond microelectrodes have been found to provide superior detection figures of merit, as compared to carbon fibers in terms of linear dynamic range, limit of detection, response variability and stability (16). There are only a few reports describing the preparation and basic electrochemical characterization of diamond microelectrodes (22, 26, 31, 32, 66, 67).

The first report on the preparation of a diamond microelectrode was published by Cooper *et al.* in 1998. Using sharpened tungsten wire as substrate, they produced two types of diamond microelectrodes by hot filament CVD (22). Other researchers used similar approach to produce BDD microelectrodes. For Example, Sarada *et al.* coated the end of a sharpened 50 μm diameter tungsten wire by microwave plasma CVD (68). The electrode was then inserted into a pulled glass capillary and back-filled with low viscosity epoxy. The end of the capillary was then slightly polished to expose the diamond tip. Olivia *et al.* fabricated the diamond microfiber electrode (69) by using very similar procedures described by Sarada *et al.*. The difference was in the last step, the end of the capillary was polished to expose a *ca.* 300 μm length of fiber to form the microfiber electrode instead of just a diamond tip exposure to form a microdisk electrode. Xie *et al.* pre-sealed a 25 μm diameter tungsten wire into a quartz capillary and then polished the capillary to expose the end of the wire for diamond growth. A disk-shaped microelectrode with about 25 μm in diameter was formed by using hot filament CVD (24). Basu *et al.* described the preparation of a conical shaped BDD microelectrode using a tungsten wire (130 μm diameter, 6cm length) as the substrate by microwave plasma CVD (70). Both ends of the tungsten wire were sheathed in quartz capillaries and insulative diamond was deposited on the exposed length of the tungsten wire. The diamond coated microelectrode was sealed in a glass capillary and insulated by a layer of photoresist. The glass capillary was then etched off in diluted HF solution to obtain a diamond tip. Recently, Holt *et al.* reported the fabrication of disc- and hemi-spherically-shaped BDD ultramicroelectrodes 1–25 μm in diameter (31). Electrically-conducting diamond was deposited on sharpened and pre-treated tungsten wires by hot filament CVD. The microelectrodes were insulated with nail varnish to produce the hemispherical architecture. To produce the disc shape, the microelectrode was completely coated with epoxy followed by a light polish to expose the diamond tip. It was also found that nail varnish or epoxy showed good insulation, but that microelectrodes insulated with

electrophoretic paint frequently lead to formation of pinholes (71). Suzuki *et al.* also successfully fabricated BDD microelectrodes with 5 μm diameter by MPCVD following procedures similar to Sarada *et al.* (26). Figure 2 shows the scanning electron microscopy images for several BDD microelectrodes fabricated by different groups.

Different from other groups, Swain group most often used Pt wire to prepare BDD microelectrode by microwave plasma-assisted CVD (16, 32, 33, 66). 25 and 10 μm diameter Pt wires are used but 76 and 40 μm diameter wires are routinely employed for biological work. Details of the approach used are given here: The Pt wire was first etched electrochemically in 1 M KOH to form a conical shape. An etching solution containing 7.0 g of CaCl₂·H₂O in a mixture of 20 mL of ultrapure water or 20 mL of acetone (33, 72). A 1.4 cm long piece of Pt wire (76 μm diam) was used. Both ends of the wire were sharpened so that two electrodes could be made from one wire. The end of the wire was immersed to a depth of 1 to 2 mm and positioned in the center of four connected carbon rod counter electrodes during etching. An AC polarization of 12 V (60 Hz) was applied between the wire and the counter electrodes using a variable autotransformer. The etching procedure lasted for approximately 5 s until gas evolution visibly ceased at the tip.

The etched wire was conically-shaped near the end and cylindrically-shaped above. Prior to diamond deposition, the sharpened wire was ultrasonically cleaned in acetone (10 min) and ultrasonically seeded (30 min) in a diamond powder suspension (5 nm particles, *ca.* 20 mg in 100 mL of ethanol). In order to prevent damage to the sharpened ends, the wire was cleaned and seeded while vertically suspended in the agitated solution. During the seeding process, the surface was scratched by the diamond particles with some particles getting embedded. Both the scratches and the embedded particles likely serve as the initial nucleation sites for film growth. A high instantaneous nucleation density is desired because this leads to the formation of a continuous film in the shortest time with a low nominal thickness. A thin film of boron-doped diamond was then deposited on the sharpened, cleaned and seeded wire. The pretreated Pt wires were mounted horizontally on the top of a quartz plate in the reactor. The quartz plate was placed in the center of the reactor's molybdenum substrate stage and served to thermally isolate the wires. The thin film of boron-doped diamond was deposited with 4 ~ 5 ppm of diborane (0.1 % B₂H₆ diluted in H₂) added for doping.

The diamond microelectrode was then attached to a Cu wire with conductive epoxy. Each electrode was sealed in polypropylene after the epoxy cured (73, 74). This was accomplished by inserting the microelectrode into a pipette tip and carefully heating the tapered end using the heating coil of a micropipette puller.

4. CHARACTERIZATION OF BDD THIN FILMS

The grain size, surface morphology and surface roughness of the BDD thin films prepared from CVD

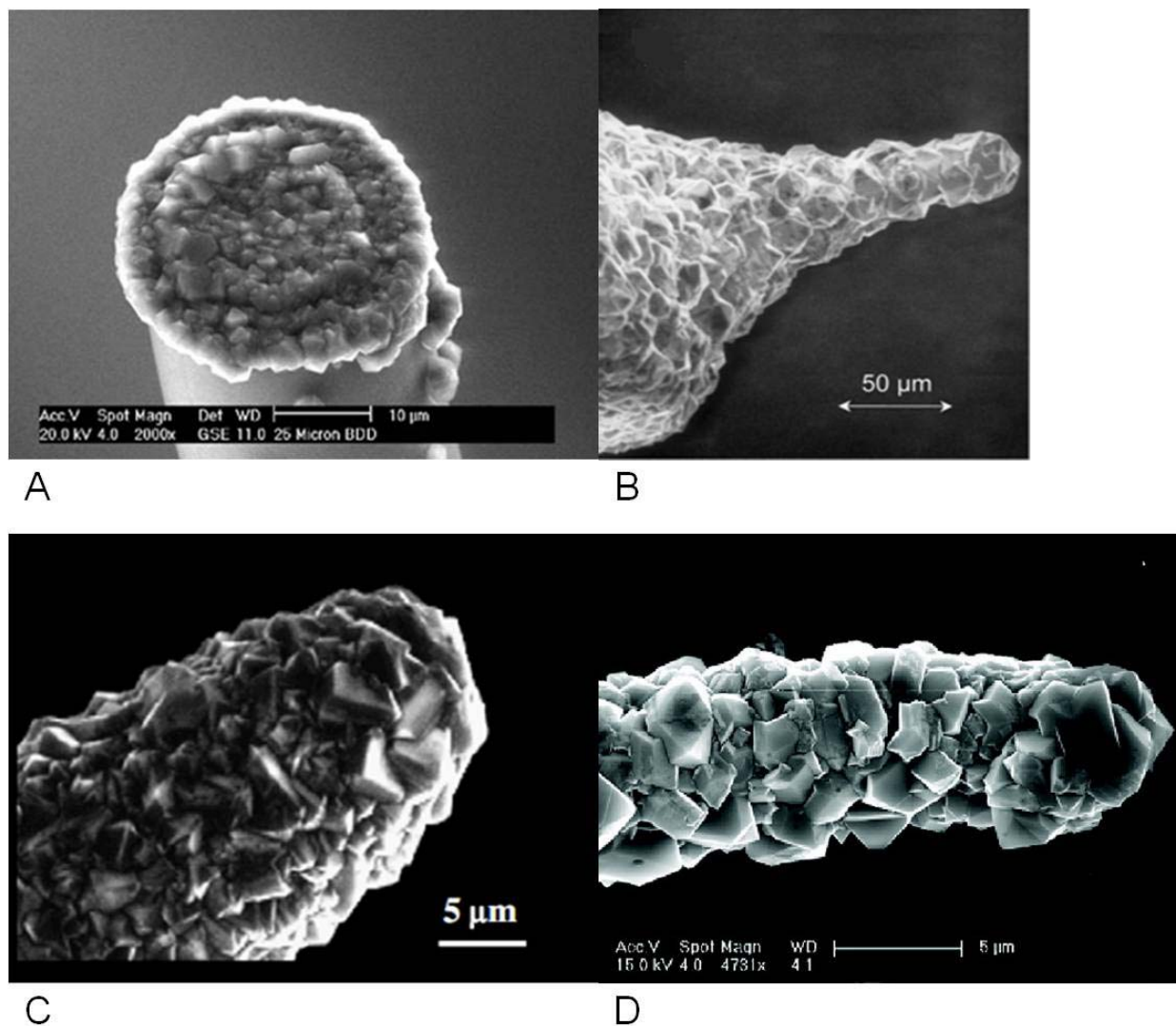


Figure 2. SEM images of selective diamond deposition onto a tungsten microelectrode (quartz insulator); final tip diameter, 35 μm (A), microcrystalline BDD growth on nanodiamond seeded tungsten wire, 10 h growth (B), the tip of a 25 μm Pt wire covered with a BDD film (C) and BDD deposition on a tungsten wire with tip diameter around 5 μm (D). Reproduced with permissions from refs (24, 31, 32, 26).

depend strongly on growth conditions. During the CVD process, sp^2 or amorphous carbon tend to be formed in the grain boundaries and defects. Therefore, the quality of BDD thin film varies from growth to growth and need to be checked or characterized. Generally, scanning electron microscopy (SEM) can be used to probe the morphology of BDD thin films such as grain size, microcrystalline orientation and surface coverage (75); atomic force microscopy (AFM) and conductive probe AFM (CP-AFM) can reveal the grain size, surface morphology, surface roughness of BDD films due to their high vertical resolution (76, 77), especially, CP-AFM is useful for investigating the electrical properties of BDD films with high spatial resolution (78-80); Raman spectroscopy is the most powerful and widely used characterization tool for diamond and amorphous carbon films because of its ability to distinguish between vibrational modes (phonons) of sp^3

and sp^2 bonding configurations (56, 81-85). These are the most useful tools for the characterization of BDD thin films. Other methods are also used for special purposes. X-ray diffraction (XRD) analysis has been used to reveal evidence for the microstructure of BDD film (86-88). For example, Zhang *et al.* studied the crystal structure of boron-doped micro- and nanocrystalline diamond films deposited by wafer-scale hot filament chemical vapor deposition by XRD and found that the microcrystalline films have a preferred (111) texture, while the nanocrystalline films exhibit (220) texture (88). X-ray photoelectron spectroscopy (XPS) is a special tool used to probe the elemental composition of the diamond surfaces (89). The atomic concentration ratio can be estimated from the peak area and the sensitivity factor of the atoms assigned from XPS (90, 91). Additionally, scanning tunneling microscopy (STM) (92), ^{11}B NMR (93, 94),

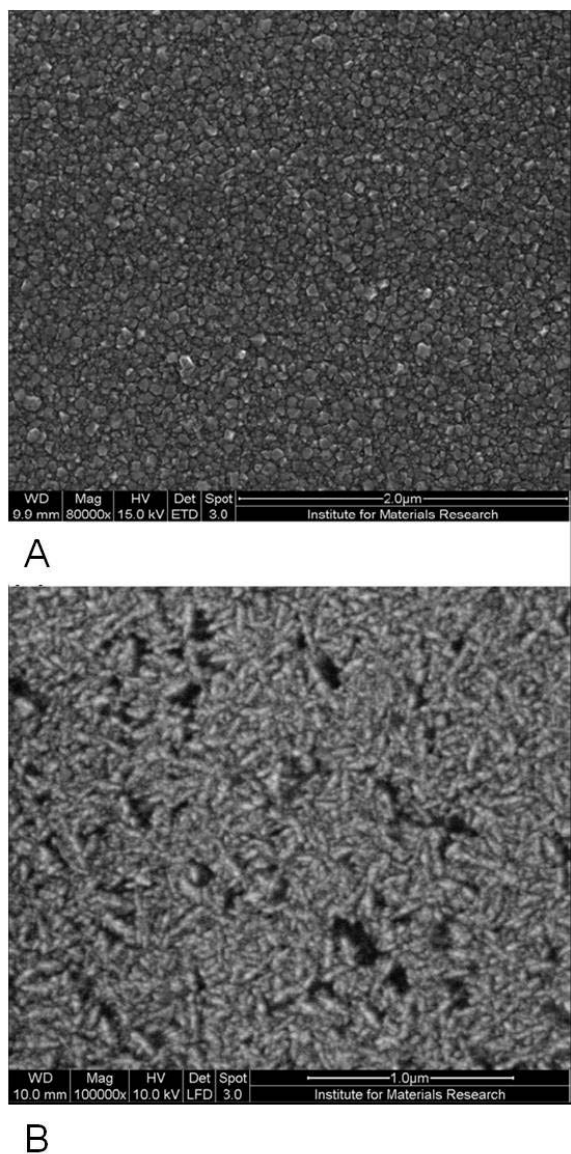


Figure 3. SEM images of a) nanocrystalline diamond and b) ultrananocrystalline diamond. Reproduced with permission from ref (75).

secondary ion mass spectrometry (SIMS) (95), cathodoluminescence (95-98), and chemiluminescence (82, 99, 100) are also used for characterization of BDD thin films.

Electrochemical characterization is important for BDD films used in electrochemistry. For carbon electrodes, the heterogeneous electron-transfer rate constant is known to be strongly influenced by the amount of exposed edge plane on sp^2 carbon electrodes (i.e., electronic properties), but weakly influenced by the oxygen functionalities terminating the edge plane carbon atoms (101-103). Surface cleanliness is also important as are the electrolyte type and concentration (103). These features can be characterized by choosing different electrochemical probes

such as $Fe(CN)_6^{3-/4-}$, $Ru(NH_3)_6^{3+/2+}$, $IrCl_3^{3-/4-}$, $IrCl_6^{2-/3-}$, $Fe^{3+/2+}$ and methyl viologen, etc.

4.1. Scanning electron microscopy

Figure 3 shows representative examples for UNCD and NCD (75). It is clear that the UNCD film consists of small carbon particles, more or less spherical in shape. These particles are actually aggregates of diamond grains (14, 58, 62). The small particle morphology is typical of films deposited from an Ar-rich source gas mixture and results from a high renucleation rate during growth (59-62). The relatively smooth morphology is maintained regardless of the film thickness. On the other hand, the NCD film shows a much greater level of faceting. Both primary and secondary growths are evident. This faceting is typical of films deposited from H_2 -rich CH_4/H_2 source gas mixtures and results from a relatively low renucleation rate during deposition. In this mode of film growth, initial nucleation events on the substrate create diamond crystals that grow three-dimensionally until the grains coalesce at thicknesses between 10 and 30 nm. Competitive growth exists between the crystals which results in a columnar texture in the growth direction.

4.2. Conductive Probe AFM (CP-AFM)

CP-AFM is a more powerful tool than AFM for investigation of BDD surface. It is one such technique that is useful for investigating the electrical properties of conductors and semiconductors with high spatial resolution (104, 105). Both nanometer electrical characterization and topographic imaging are provided by CP-AFM. The technique usually employs a metal-coated (Pt or Au) cantilever-tip assembly that functions as both a scanning electrical contact and force sensor. Metal wire probe tips can also be used (106). As a result, direct measurements of I-V curves at specific topographical sites on the sample are possible.

CP-AFM has been used to probe the conductivity across BDD thin-film electrodes with different boron-doping levels (78), and undoped diamond films (107). The general observation, at least in some of the work, is that the electrical conductivity is variable across polycrystalline diamond with a strong dependence on the grain orientation, fraction of grain boundary, and boron-doping level (13, 58, 108).

Figure 4 shows the topographical (A) and conductivity (B) maps of a boron-doped nanocrystalline film (NCD) deposited from an H_2 -rich source gas mixture. In the topographical map, a few of the small crystals are evident. In the conductive map, isolated highly conductive regions are seen over the surface with most of grains exhibiting high conductivity. There are some grains and boundaries showing lower conductivity (see the grains at the middle of the upper edge and lower left corner of Figure 4A and B). One reason for the heterogeneous conductivity over the film is variability in the boron-doping in different growth sectors of the film (79, 109, 110).

4.3. Raman spectra

Raman spectra is the most widely used characterization tool for diamond and amorphous carbon

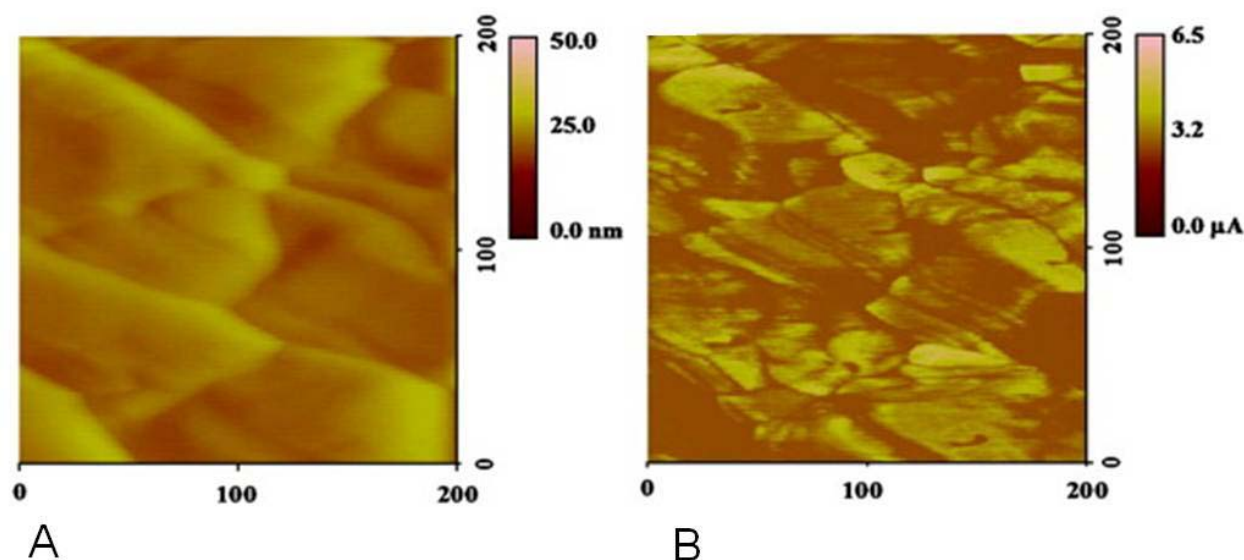


Figure 4. Topographical image (A) and (B) conductivity map of a boron-doped NCD film. Reproduced with permission from ref (65).

films because of its ability to distinguish between vibrational modes (phonons) of sp^3 and sp^2 bonding configurations (56, 81-85). The interpretation of Raman spectra is fairly straightforward for characterizing crystalline diamond and graphite, but the interpretation gets more complicated for mixed sp^2 - sp^3 bonded materials due to differences in the Raman scattering cross-section (56, 81, 84, 85, 111). The spectra for nanocrystalline diamond films are quite distinct from the typical spectrum for single crystal diamond, which consists of single, narrow band at 1332 cm^{-1} (81, 82). As shown in Figure 5 (A), the spectrum for the UNCD film has three primary peaks at 1155 , ~ 1345 (broad) and 1550 cm^{-1} with additional scattering intensity at 1470 cm^{-1} . This spectrum is very characteristic of UNCD films deposited from Ar-rich mixtures (58, 61, 62, 112).

The diamond one-phonon line at 1331 cm^{-1} for UNCD film is not as prominent as it is for single crystal diamond. It is actually hidden by the strong scattering of sp^2 carbon components in the film. Due to resonant enhancement, most of the scattering intensity comes from the sp^2 bonded carbon in the grain boundaries near 1360 cm^{-1} , i.e. the so-called D-line of disordered sp^2 carbon (81, 84, 85).

The broad peak at 1550 cm^{-1} is attributed to the nondiamond sp^2 -bonded carbon in the grain boundaries. It is also possible that the sp^2 -bonded carbon scattering results from material at the interface between the diamond film and the Si substrate (85). The 1155 cm^{-1} peak is often used as a diagnostic feature of nanocrystalline sp^3 -bonded diamond mainly because of its presence in the spectrum of nanocrystalline diamond films (58, 61, 62, 83, 111). This assignment is based on the fact that this peak is near a maximum in the vibrational density of states at *ca.* 1200

cm^{-1} (61, 83, 111). The most seminal work understanding the origin of these two peaks has come from Ferrari and Robertson, who concluded that the scattering at these two frequencies is not due to C-C sp^3 vibrations but rather to scattering from trans-polyacetylene oligomers (C-C sp^2 vibrations) of different conjugation lengths in the grain boundaries (111).

The Raman spectrum for the heavily boron-doped NCD film is very different from that for the UNCD film. In Figure 5 (B), the diamond one-phonon peak is downshifted to 1312 cm^{-1} , attenuated and superimposed on a broad scattering peak centered at 1215 cm^{-1} . There is also a weakly intense peak at 1010 cm^{-1} and a relatively intense peak at 477 cm^{-1} . This spectrum is characteristic of heavily boron-doped single and polycrystalline (microfaceted) diamond films (109, 113, 114).

Figure 5 (C) shows the Raman spectra for the microcrystalline diamond film from a highly doped diamond microelectrode (68). Different from the spectra of NCD and UNCD, a single, narrow peak at 1332 cm^{-1} indicates the high quality of the single crystal diamond. The absence of a peak at around 1600 cm^{-1} represents that the microcrystals are free from nondiamond carbon impurities. And the absence of a peak at around 1200 cm^{-1} indicates there is little contribution from disordered diamond. The shoulder before the sp^3 carbon peak is attributed to the high boron doping concentration.

4.4. Electrochemical characterization

Four most often chosen redox systems used to evaluate the electrochemical behavior of the BDD electrodes are $\text{Fe}(\text{CN})_6^{3-/4-}$, $\text{Ru}(\text{NH}_3)_6^{3+/2+}$, $\text{IrCl}_6^{2-/3-}$ and methyl viologen (101-103). $\text{Fe}(\text{CN})_6^{3-/4-}$ was used as a probe because the electrode reaction kinetics for this couple

Boron-doped diamond microelectrodes for *in vitro* measurements

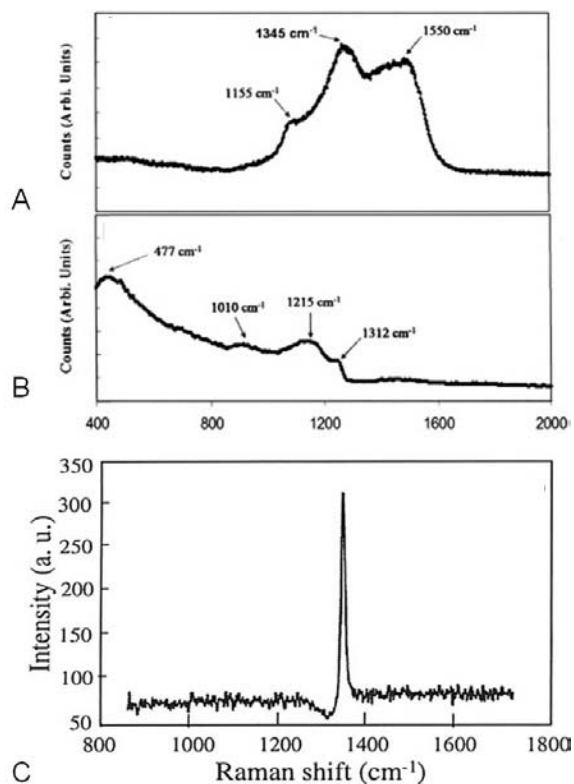


Figure 5. Raman spectra for boron-doped (A) UNCD (B) NCD films (C) microcrystalline BDD film. Reproduced with permission from refs (65,68).

are strongly influenced by the amount of exposed edge plane on sp^2 -bonded carbon, as well as the surface cleanliness (13, 103, 115-117). Therefore, its heterogeneous electron-transfer rate constant is quite sensitive to the surface cleanliness and chemistry of sp^2 and sp^3 carbon electrodes (6, 101, 102, 118). This redox system often behaves anomalously on carbon electrodes and should not be considered typical outer-sphere. The electrochemical kinetics of $Fe(CN)_6^{3-/4-}$ has been studied extensively. For example, studies show that there are several factors that can influence the electrode kinetics at metal and sp^2 carbon electrodes. First, the rate constant is strongly influenced by the fraction of edge plane exposed on sp^2 carbon electrodes (i.e., electronic properties), but relatively insensitive to the surface oxygen functionalities terminating the edge plane carbon atoms as long as a thick, anionically charged oxide film is not present (101-103). Second, surface cleanliness is important, as are the electrolyte type and concentration (119, 120). For example, the involvement of specifically adsorbed cations (e.g., K^+) through a possible surface-bridging interaction has been proposed (119, 120). The rate of reaction increases with electrolyte composition in the order of $LiCl < NaCl < KCl$ (119). At the 1 mol/L electrolyte concentration, the rate is a factor of ~ 10 higher in KCl than in LiCl at both gold and glassy carbon electrodes (101, 102). Third, adsorbed monolayers on sp^2 carbon electrodes can decrease the rate of reaction. The McCreery group observed an increase in ΔE_p from 5 to 140 mV after modification of the polished

glassy carbon surface with adsorbed monolayers (121). The level of increase depends on the type and coverage of the adsorbate.

Different from sp^2 -bonded carbon electrodes, the physicochemical properties of boron-doped diamond strongly influence the electrode kinetics of $Fe(CN)_6^{3-/4-}$. ΔE_p of $Fe(CN)_6^{3-/4-}$ is very sensitive to the surface termination with the smallest ΔE_p observed at the clean, hydrogen-terminated surface. After oxygen termination, ΔE_p increases by over 125 mV but is reversibly reduced to the original value after removal of the oxygen functionalities by hydrogen plasma treatment (119). The sensitivity of the electrode kinetics to surface oxygen at diamond is in sharp contrast to the minor effects these functionalities have on the response at sp^2 carbon electrodes.

The $Fe(CN)_6^{3-/4-}$ rate constant is also sensitive to the electrolyte composition and ionic strength with the largest values observed in KCl and the smallest in LiCl. This dependence is presumed to result from the formation of a dimeric species consisting of both the oxidized and reduced forms of the anion coupled through a bridging cation and stabilized by some specific surface interaction (122). However, the difference at the 1 mol/L concentration level is only a factor of 2-3 rather than 10, as is the case for metal and glassy carbon electrodes (5, 108, 117, 123, 124). All the evidence at sp^2 carbon and diamond electrodes suggests the involvement of a clean, non-oxide surface site.

$Ru(NH_3)_6^{3+/2+}$ involves simple electron transfer at most electrodes including diamond and sp^2 carbon (101-103, 125). The electrode kinetics for $Ru(NH_3)_6^{3+/2+}$ are relatively insensitive to the surface microstructure, surface oxides, and adsorbed monolayers on sp^2 carbon electrodes (103). The electron transfer rate constant of this redox couple is insensitive to surface modification, which strongly implies that electron transfer does not depend on an interaction with a surface site or functional group (124). The most important factor affecting the rate of reaction is the electronic properties of the electrode, specifically the density of electronic states near the formal potential of the redox system.

For metal and glassy carbon electrodes, a low density of electronic states is seldom an issue. However, for semiconducting/semimetallic diamond, the potential dependent electronic density of states is an important factor governing the response. This is why ΔE_p increases at boron-doped diamond thin film electrodes with decreasing boron doping level (123, 126). ΔE_p for 10 ppm diamond film was 56 mV and increased to 78 mV when the doping level decreased to 0.1 ppm. The nearly reversible response indicates that there must be a sufficient density of electronic states present within the band gap at this potential. The evidence suggests that the boron-doping level and the chemisorbed hydrogen are the most important factors controlling the density of electronic states in this potential region.

Similar to $Ru(NH_3)_6^{3+/2+}$, $IrCl_6^{2-/3-}$ involves simple electron transfer at most electrodes including diamond (103) and sp^2 carbon (101-103, 125). The k_{app}^0 is

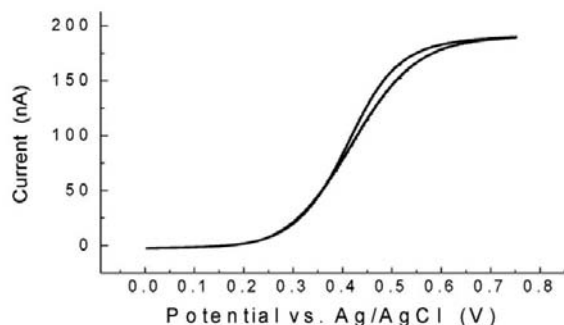


Figure 6. Cyclic voltammetric *i*-*E* curves for boron-doped diamond microelectrodes (25 μm) in 1 mM $\text{K}_4[\text{Fe}(\text{CN})_6]$ plus 1 M KCl at a nail polish-insulated microelectrode (25 mV/s). Reproduced with permission from ref (32).

relatively insensitive to the surface microstructure, surface oxides, and adsorbed monolayers on sp^2 carbon electrodes (126). Surface cleanliness is important, although to a lesser degree than for $\text{Fe}(\text{CN})_6^{3-/4-}$. The most influential factor is the electronic structure of the electrode.

Methyl viologen also involves simple electron transfer at diamond and most other electrodes (121, 127, 128). The k_{app}^0 at diamond is relatively insensitive to surface oxides, grain boundaries, defect density, and the presence of nondiamond carbon impurities. Like $\text{Ru}(\text{NH}_3)_6^{3+/2+}$, the most important factor influencing the rate is the density of electronic states at the formal potential. Surface cleanliness and electronic effects appear to be the most influential factors determining the rate, and this redox system behaves as outer-sphere (80).

During preparation, cracks or defects are more easily formed on BDD microelectrode because of the size and shape of the electrode. It's difficult to find these cracks or defects by SEM or Raman. Electrochemical characterization such as cyclic voltammetry is extremely powerful on revealing any defects on the electrode. In addition, by using cyclic voltammetry, the effective area of the microelectrode can be determined, which is very critical in the application of BDD microelectrode for analytical purpose. Therefore, it's necessary to conduct electrochemical characterization before the BDD microelectrode can be used for *in vitro* biological measurement as a sensor. The electrochemical behavior of microelectrode is very different from the macroelectrode. The microelectrode mentioned in this paper means the electrode has at least one dimension smaller than the scale of the diffusion layer developed in readily achievable experiments, although there is no broadly accepted definition of a microelectrode at present. The microelectrode electrochemical performance is obviously influenced by its shape. The most commonly used shapes for microelectrode are discal, spherical, hemispherical and cylindrical shape. At long times, where the diffusion layer thickness is large compared to the critical dimension, the current at any microelectrode approaches a steady state or a quasi-steady state, which is called the limiting current and can be expressed as (129):

$$i_{ss} = nFmC^*$$

where m is a mass-transfer coefficient, which functional form depends on geometry of the microelectrode.

As mentioned previously, BDD microelectrode has a variety of geometries and, consequently, different current characteristics. For BDD microelectrode with a shape of combining cylinder and cone, for example, the limiting current is given by (32):

$$i_{ss}^2 = i_{ss}^{\text{cylinder}} + i_{ss}^{\text{cone}} \quad \text{where } i_{ss}^{\text{cylinder}} = \frac{2nFADC^*}{r \ln \tau}$$

$$i_{ss}^{\text{cone}} = 4nFDC^*r(1 + qH^p) \quad \text{and } \tau = \frac{4Dt}{r^2}$$

In the above equations, n is the number of electrons transferred per equivalent, F is the Faraday constant, which is 96485 C/mol, A is the electrode area (cm^2), D is the diffusion coefficient of the analyte (cm^2/s), C^* is the bulk concentration of the analyte (mol/cm^3), r is the cylinder or cone radius (cm), $q = 0.30661$, $p = 1.14466$, and H is the aspect ratio h/r where h is the height of the cone (cm). The measurement period, t (s), is the time of the forward voltammetric scan. The surface area of a cone is related to its aspect ratio according to the equation $A = \pi r^2(H + 1)^{1/2}$ (32, 130). Therefore, exposed electrode area can be determined from the measured mass transport-limiting current.

Figure 6 shows a typical cyclic voltammetric *i*-*E* curves for a BDD microelectrode (25 μm) in 1 mM $\text{K}_4\text{Fe}(\text{CN})_6$ and 1 M KCl solution with a scan rate of 25 mV/s. Quasi-steady state current on BDD microelectrode is observed in this voltammogram. The $E_{1/2}$ value is around 400 mV vs. Ag/AgCl, which reflects the slow electron transfer kinetics for diamond electrode (131). This voltammogram indicate that the electrode surface is clean, no blemish or crack.

5. APPLICATION OF BDD ELECTRODE FOR BIO-SENSING AND *IN VITRO* MEASUREMENTS OF BIOMOLECULES

5.1. Continuous amperometry

With continuous amperometry, the potential of the working electrode is adjusted to a value at which the analyte of interest can be electrolyzed within the mass transfer-limited region. The current that flows through the working electrode is measured and its amplitude is related to the diffusive overflow of analyte in the vicinity of the working electrode. Since the potential is held at a certain value, the background current is low and therefore, the excellent temporal resolution and high sensitivity provided by amperometry allows measurement in real time to be made. This technique has been successfully applied to the measurement of neurotransmitters from tissues and single cells, such as adrenal chromaffin cells (132-134). The limit of detection of this technique can be as low as attomole and zeptomole for measurements of neurotransmitters released from single synaptic vesicles (135). However, this technique measures the fluxes of all electroactive species

to the electrode surface and thus lacks sufficient selectivity for many applications.

5.1.1. Norepinephrine measurement from rat mesenteric artery

Norepinephrine (NE) is the principal neurotransmitter released from sympathetic nerves. It is a member of catecholamine family and is secreted by the adrenal medulla and sympathetic nerve endings. NE release from sympathetic nerves supplying the cardiovascular systems causes vasoconstriction, increased heart rate, blood pressure, and it mobilizes glucose stores in the liver and skeletal muscle (136). NE is electroactive and can be detected as an oxidation current based on a 2 electron/2 proton redox reaction with quinone as the final product. Pioneered by Gonon and coworkers in 1993, the electrochemical method with a carbon fiber microelectrode was applied to detect NE released in the sympathetic nervous system (137). Since then, this technique has been widely used to study neurotransmitter release kinetics *in vitro* and *in vivo* (133, 138, 139). Park *et al* for the first time applied boron-doped diamond microelectrode to the *in vitro* measurement of NE released from the sympathetic nervous system in rat mesenteric arteries (23, 33, 66). The BDD microelectrode used in their work was fabricated by microwave-CVD and a sharpened 76 μm platinum was employed as the substrate to form a conical shaped geometry. In their preliminary study, the authors compared the response sensitivity, precision and stability of a diamond microelectrode with a carbon fiber microelectrode for the measurement of NE by cyclic voltammetry (33). The key findings are: 1) a smaller peak shift was seen in a diamond microelectrode response for a surface-sensitive redox system, $\text{Fe}(\text{CN})_6^{3-/4-}$, after tissue and laboratory atmosphere exposure compared to a carbon fiber microelectrode; 2) a low, stable and pH-independent background current was exhibited for a diamond microelectrode compared to a pH-dependent background current from a carbon fiber microelectrode; 3) the decrease of the NE signal generated from flow injection after 4 hours tissue exposure was much less from a diamond microelectrode (7%) compared to that from a carbon fiber microelectrode (30%). The authors attributed the deactivation and fouling resistance of diamond microelectrode to its hydrophobic, H-terminated sp^3 -bonded carbon surface and the absence of extended π -electron system and surface oxides, which may also be the reason for the sluggish electrode reaction kinetics for catechol and catecholamine redox chemistry on its surface. The bare diamond without a protective ionomer coating provided excellent response sensitivity and stability for the *in vitro* measurement of NE in a biological environment.

The authors further applied this technique together with the video microscopy technique to a more comprehensive study for the *in vitro* monitoring of endogenous NE release and the effect of NE on the contractile response of a rat mesenteric artery (23). The set-up for the diamond microelectrode, electrical stimulator, the rat tissue, the current-time profile and the corresponding blood vessel contraction are shown in Figure 7. NE release was elicited by electrical stimulation and is

frequency dependent. The detection potential was set up at +0.8 V vs. Ag/AgCl reference electrode. The current that flows through the working electrode was measured and its amplitude was related to the diffusive overflow of NE from multiple neuroeffector junctions in the vicinity of the working electrode. The release of NE from the sympathetic nerves was verified by using a sodium channel antagonist, tetrodotoxin, which can block nerve conduction and therefore abolish NE release. Combined with related drugs, the authors studied the frequency-dependent release and clearance of NE, as well as the function of NE on the contractile response of the rat mesenteric arteries. The results demonstrate that continuous amperometric monitoring of NE with a BDD microelectrode and video imaging of vascular tone can be used to study the real time local measurement of the temporal relationship between nerve-stimulated NE release and arterial constriction. The NE release and clearance mechanisms can therefore be investigated by using this technique coupled with drugs. The key was the use of a diamond microelectrode because of the excellent response sensitivity, reproducibility, and stability it provided.

5.1.2. Serotonin (5-HT) measurement from guinea pig and rabbit intestinal mucosal layer, and rhesus monkey lymphocytes

Serotonin (5-hydroxytryptamine, 5-HT) is an important signaling molecule in the gastrointestinal tract (36). Over 90% of the body's 5-HT is synthesized and stored in the enterochromaffin (EC) cells located in the mucosa of the gut (140). 5-HT is electroactive and can be oxidized by a one electron reaction (141, 142). Its measurement in the intestinal mucosa was accomplished using electrochemical method with a carbon fiber microelectrode positioned on the mucosa of guinea pig ileum maintained *in vitro* (143). Using this approach, it has been possible to monitor 5-HT release from a few EC cells in real time. However, the oxidation of 5-HT can form a radical cation, which deprotonates to form a serotonin radical that reacts with other molecules to form dimers or trimers absorbed onto the surface of the carbon fiber electrode. Therefore, the electrochemical monitoring of 5-HT *in vitro* or *in vivo* is often hindered by the electrode fouling and signal loss (28, 144) resulting from this insulating film on the carbon fiber surface. Recently, Patel *et al* and Zhao *et al* successfully detected 5-HT from the EC cells of the intestinal mucosal layer in the guinea pig using a BDD microelectrode (25, 145, 146). The conical shaped BDD microelectrode was fabricated using the same method described above. The detection potential of the working electrode was set up at +0.7 V vs. Ag/AgCl and the local 5-HT overflow was measured as an oxidation current. The endogenous 5-HT overflow was elicited by both mechanical and electrical stimulation. The 2.5 times increased current caused by serotonin transporter (SERT) inhibitor, fluoxetine (1 mM), verified that the oxidation current was associated with 5-HT. Both 5-HT and the paracrine hormone, melatonin, were detected in the extracellular solution. The key to the accurate and stable measurements of 5-HT is the properties of the BDD

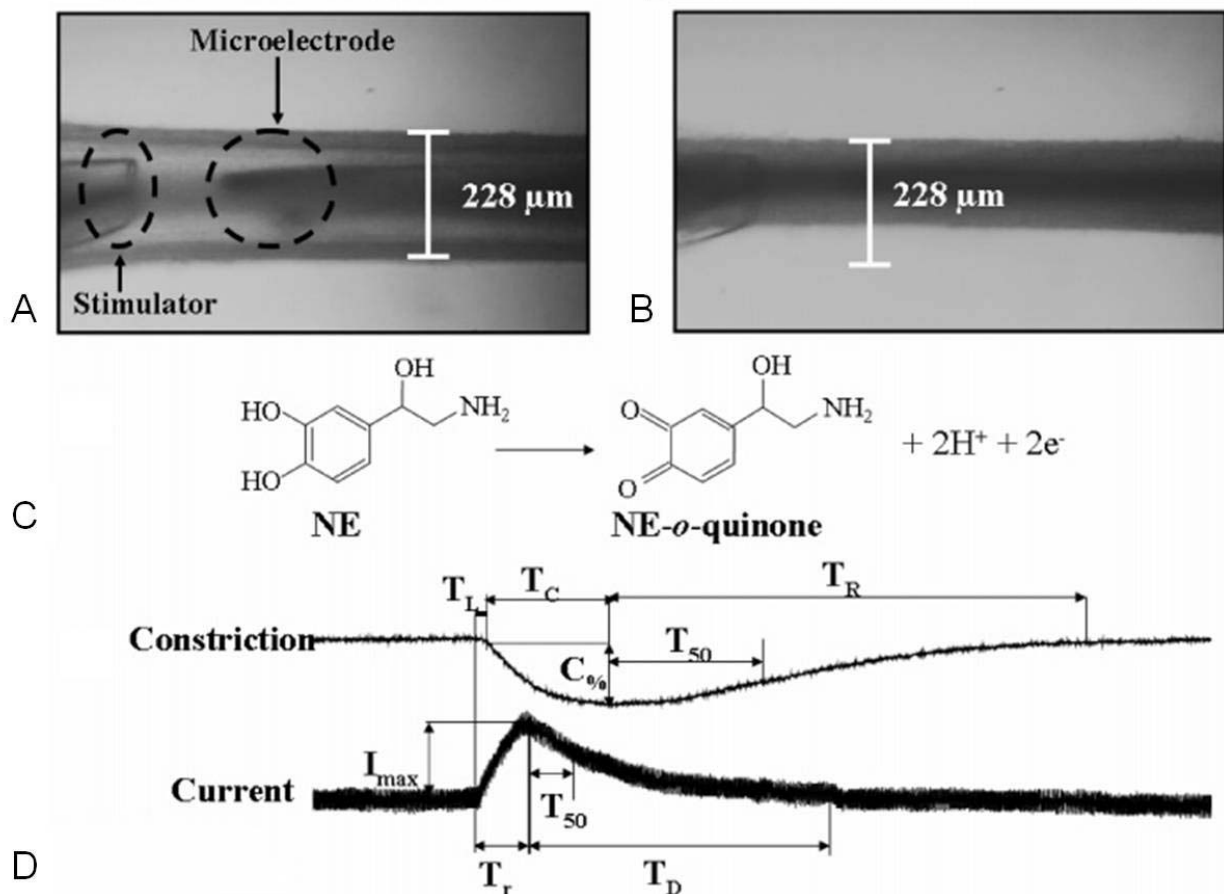


Figure 7. Video image showing the setup for *in vitro* measurement of NE with a diamond microelectrode from a mesenteric artery and the current time response curve. Video micrographs showing a mesenteric artery (A) before and (B) after a 20-Hz electrical stimulation (60 pulses with a 0.3-ms pulse width). The bipolar stimulator electrode and the diamond microelectrode, both positioned at the artery surface, are evident in (A). The NE oxidation reaction mechanism is shown in (C). Characteristic contractile (top) and NE oxidation current (bottom) response transients in response to a 20-Hz stimulation are presented in (D). Detection potential at 800 mV. Several numerical parameters are obtained from these curves, including the maximum oxidation current, I_{max} ; the current rise time, T_r ; the time required for current decay to 50% of the maximum, T_{50} ; the time required for full current decay, T_D ; the percent constriction, $C_{\%}$; the time required to reach full constriction, T_C ; the time required for full vessel relaxation, T_R ; and the latency period prior to the onset of constriction, T_L . Reproduced with permission from ref (23).

microelectrode minimize fouling that is observed on the carbon fiber or noble metal microelectrodes during *in vitro* measurements (144, 147). Due to absence of the extended π -electron system and a lack of polar carbon-oxygen surface groups, only some minor electrode fouling was seen for diamond and the stabilized response enabled the accurate recording of 5-HT *in vitro*. The important finding from their work is continuous amperometry coupled with a BDD microelectrode provides accurate and stable measurements of 5-HT release, allowing physiological studies of EC cell to be conducted.

In the following study conducted by Bian *et al*, BDD microelectrodes were utilized to investigate the 5-HT release from EC cells in the intestinal mucosa of neonate

and adult guinea pigs (148). The authors compared the 5-HT oxidation current with and without the SERT inhibitor, fluoxetine (1 mM), from neonate and adult guinea pigs EC cells. Fluoxetine potentiated oxidation currents in adult but not neonatal tissues indicating that the SERT function is age dependent. Combined with immunohistochemical and Western blot measurements, the results suggested that functional SERT expression is not yet developed and therefore, there is no mechanism for clearance of 5-HT released by EC cells in the neonatal intestine.

In a separate study, Patel used the BDD microelectrode simultaneously recorded both 5-HT and melatonin overflow from EC cells in the mucosa of rabbit ileum (149). Melatonin is a paracrine signalling molecules,

which may also be synthesized by EC cells and has influence on intestinal muscles (150). Electrochemical measurements were carried out using amperometric detection, where the potential of +0.7 V vs. Ag/AgCl was utilized for the detection of 5-HT, and a potential of +0.8 V vs. Ag/AgCl was used to oxidize both 5-HT and melatonin. The oxidation peak amplitudes were calibrated by the flow injection analysis. The key finding of this work is that 5-HT and melatonin can be simultaneously monitored in real time by using a BDD microelectrode and they may be modulated by different mechanisms in the mucosa EC cells of rabbit ileum.

Singh and coworkers just published their work on the detection of 5-HT in lymphocytes from adult rhesus monkeys using BDD microelectrodes (151). By doing that, they intended to investigate variations in 5-HT transport in primary lymphocytes associated with the rhesus 5-HT transporter gene-linked polymorphism (rh5-HTTLPR). They first compared the response signals of 10 μM 5-HT solutions from both 70 μm cylindrical BDD microelectrodes and 30 μm cylindrical carbon fiber microelectrodes. The average 5-HT oxidation half-wave potential ($E_{1/2}^{\text{ox}}$) was 0.5 ± 0.008 V at the BDD microelectrode and 0.3 ± 0.005 V at the carbon fiber microelectrode, which is consistent with that a more sluggish electrode reaction kinetics happens on the BDD microelectrode surface. However, the signal to background ratio was significantly higher at the BDD microelectrode than that at the carbon fiber microelectrode. The absence of redox-active ionizable surface groups and lower concentrations of internal charge carriers in BDD microelectrode lead to lower background currents and noise. According to the 5-HT signal – applied detection potential plot, the oxidative potential of + 0.8 V vs. Ag/AgCl at BDD microelectrode and + 0.55 V vs. Ag/AgCl at carbon fiber microelectrode were applied for 5-HT detection. Under these condition, the responses to 1 μM 5-HT by BDD microelectrode, bare carbon fiber microelectrode and Nafion-coated carbon fiber microelectrode were further compared. BDD microelectrode showed significantly higher signal-to-noise, signal-to-background ratios, better limit of detection, and minimum fouling in both 10 μM 5-HT solution and lymphocytes compared to those of Nafion-coated or bare carbon fiber microelectrodes. Furthermore, the original signal for BDD microelectrode could almost be fully recovered by the treatment of isopropanol after fouling. BDD microelectrodes were then used for the *in vitro* measurement of 5-HT in lymphocytes from adult rhesus monkeys because of their excellent response sensitivity and stability. Combined with the use of 5-HT selective reuptake inhibitor, paroxetine (100 nM), the authors concluded that there was reduced 5-HT uptake rates in lymphocytes from adult rhesus monkeys carrying the short allele of the 5-HTTLPR and lymphocytes could possibly be used as peripheral biomarkers for investigating genetic or pharmacologic alterations in 5-HT transporter function. The use of BDD microelectrodes, in contrast to carbon fiber microelectrodes used previously in the brain study, enabled these high-sensitivity and high-resolution measurements.

5.1.3. Nitric oxide measurement from guinea pig ileum

Nitric oxide (NO) is a gaseous signaling molecule and an inhibitory neurotransmitter that causes relaxation of the muscle layers in the gut (152). It plays a very important role in the gut function. NO release from myenteric neurons was measured indirectly by measuring drug or electrical stimulation induced relaxation of smooth muscle (153). Very few techniques can be used for the real-time measurement of NO near the sites of release. NO is electrochemically active at many electrodes and can be detected as an oxidation current which is proportional to the amount of NO at the electrode surface. Electrochemical techniques with a carbon fiber microelectrode or a polyion-coated gold electrode have been used to detect NO release in the brain slice (154-156). Patel *et al* for the first time described the monitor of NO release from myenteric neurons *in vitro* in isolated segments of guinea pig ileum using continuous amperometry with a BDD microelectrode (157). The diameter of BDD microelectrode is around 40 μm and the applied potential determined by differential pulse voltammetry for NO measurement was +1 V vs. Ag/AgCl. Nicotine (1 μM) superfusion was used to induce the release of NO from the longitudinal muscle myenteric plexus of guinea pig ileum by activating nicotinic acetylcholine receptors expressed by myenteric neurons and myenteric nerve endings. Due to the resistance to fouling, BDD microelectrodes showed 4 times higher signal of NO induced by nicotine (1 μM), compared to carbon fiber microelectrodes. The most challenging part for the *in vitro* NO measurement is selectivity since there are other electroactive molecules, such as NE, 5-HT, and nitrite, which can also be oxidized at the applied potential for NO detection but cannot be distinguished by amperometry. The authors verified that the oxidation current detected by a BDD microelectrode was solely caused by NO flux by showing that 1) there was no current at +0.75 V vs. Ag/AgCl, where the oxidation of catecholamines and biogenic amines can occur, 2) the NO synthesis antagonist, N-nitro-L-arginine, almost completely abolished the oxidation current, 3) current was reduced by the NO scavenger, myoglobin. The authors then compared the difference in NO release from the myenteric plexus and circular muscle. The key finding for this work is continuous amperometry with a plain BDD microelectrode is very useful in the real-time monitor of locally produced NO and the investigation of NO signaling in the gut.

5.1.4. Histamine measurement from oxyntic glands of guinea pig stomach

Histamine is a biogenic amine involved in local immune responses as well as regulating physiological function in the gut and acting as a neurotransmitter. An important site of histamine storage and release is the enterochromaffin-like (ECL) cell of the stomach (158, 159). Histamine levels in the stomach can be monitored by microdialysis and off-line separation-based methods which are less of temporal resolution (160, 161). Bitziou *et al.* recently reported a dual-sensor method for the real-time simultaneous detection of pH changes and histamine release from oxyntic glands of isolated guinea pig stomach (162). A BDD microelectrode was used in an amperometric mode to detect histamine released from the

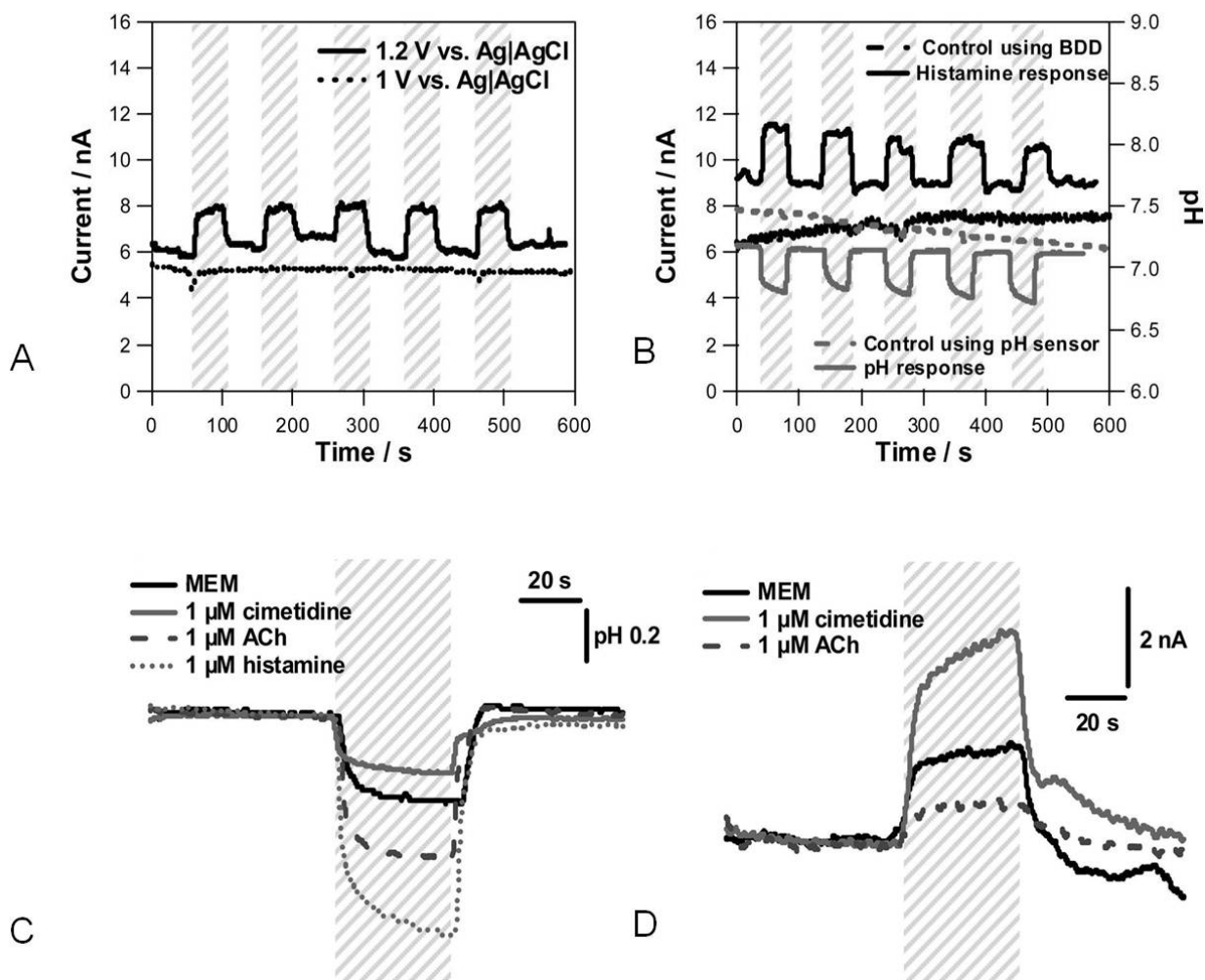


Figure 8. Experimental controls conducted for biological *in vitro* measurements and the influence of various pharmacological treatments. (A), repeated response over the tissue at a potential of 1.2 V, which is sufficient to oxidize histamine and at 1 V, which shows if any of the signal is due to catecholamines and serotonin. (B), the response obtained from the BDD and IrO₂ pH sensor with and without the tissue, showing that the responses obtained are from the isolated stomach tissue. The shaded gray box indicates the duration when the sensor is located within 1 mm over the tissue. The responses obtained before and after cimetidine (H₂ receptor antagonist), acetylcholine, and histamine treatment from the iridium oxide pH sensor are shown in (C), and in (D), the responses from the BDD microelectrode are shown. Reproduced with permission from ref (162).

ECL cell, while an iridium oxide pH microelectrode was used in a potentiometric mode to record the pH decrease associated with acid secretion. The BDD microelectrodes used in this work were fabricated by microwave-CVD technique with 40 μm platinum wires as the substrate and around 100–200 μm exposed electrode length. Differential pulse voltammogram of 50 μM histamine was obtained first for the identification of the histamine oxidation potential. Amperometric measurements using flow injection analysis were then carried out for the calibration of histamine. The *in vitro* recordings of histamine levels from the ECL cells were conducted using amperometric detection at + 1.2 V vs. Ag/AgCl. The BDD microelectrodes can sensitively, reproducibly and stably record the histamine level *in vitro*. Figure 8 shows the

responses from the dual electrodes system for *in vitro* measurements of histamine, and the signal changes as a function of pharmacological treatment. The concern of oxidation current contributed by other electroactive compounds, such as 5-HT, dopamine and nitric oxide, was eliminated by showing that there was no signal response at the potential of + 1.0 V vs. Ag/AgCl, where 5-HT, dopamine and nitric oxide can be oxidized. It also showed that there was no interference for the measurements of histamine on the BDD microelectrode with the measurements carried out on the pH electrode.

The authors then applied this dual-sensor system for probing the signaling mechanism that influences acid secretion in the guinea pig stomach. When cimetidine, a H₂

receptor antagonist, was added to the physiological buffer, there was a 2-fold increase in Δi while a significant decrease in ΔpH compared to the control. However, the increase of the current was unanticipated and the information was not sufficient to explain how the H₂ receptor antagonist regulates the level of histamine. The conclusion that acetylcholine can modulate gastric acid secretion via a neuronal mechanism was drawn based on the finding of the significantly decreased endogenous histamine current level and pH of the buffer after acetylcholine application to tissue. With the novel two-sensor-system and the pharmacological agents, the authors showed that the simultaneous measurement was physiological relevant and acetylcholine influences muscarinic receptors on the parietal cell via a direct mechanism, rather than through the ECL cell. These important findings highlight that continuous amperometry monitoring of histamine with a BDD microelectrode and the recording of pH change by an iridium oxide pH microelectrode can be very useful in obtaining the information for significant signaling mechanisms and pathways.

5.2. Fast scan cyclic voltammetry

Amperometry offers excellent temporal resolution and sensitivity, but it is typically difficult to interpret amperometric results for component mixtures. In this case, the other most often used method, fast scan cyclic voltammetry (FSCV), is a good choice. FSCV can generate a “finger print” response for each analyte, potentially allowing a distinguishable measurement in the presence of multiple components (163, 164). In FSCV, a gradually increasing or decreasing potential is applied at the working electrode with a high scan rate (> 100 V/s). When the maximum or minimum desired potential is reached, the direction of the sweep is reversed. The current flow is measured during increases and decreases in electrode potential. At a high scan rate, a relatively large background current is seen and the smaller faradaic current can only be detected after background subtraction. The occurrence of a signal peak at a particular potential reflects transient change of the local concentration of substance present at the vicinity of the working electrode. Qualitative and quantitative information can be obtained for each redox pair when different species possess different oxidation and reduction potentials (165). This technique has been applied to measurements of dopamine, NE, serotonin, and ascorbic acid especially in the central nervous system (164, 166, 167). The advantage of this technique is that different compounds can be distinguished by different position of the peaks in the voltammogram.

5.2.1. Adenosine measurement from PreBöttinger Complex in rat brain stem

Adenosine is an important neuromodulator which has an inhibitory effect in the central nervous system (37). Xie *et al* for the first time detected adenosine in a neural system *in vitro* by using a BDD microelectrode (24). The authors fabricated the non-planar, needle-like microdisk diamond microelectrodes by using hot-filament assisted

CVD fabrication technique. A tungsten microwire with a 25 μ m diameter was presealed into a pulled quartz capillary and only the tip was polished to expose the tungsten substrate for diamond deposition. The diamond microsensor was calibrated using standard flow injection analysis as well as FSCV. The FSCV potential was scanned linearly between -1.0 and +1.5 V vs. Ag/AgCl reference electrode with a scan rate of 500 V/s. The adenosine oxidation peak appeared at +1.1 V vs. Ag/AgCl reference electrode. The lowest concentration of detected adenosine shown in their work was 10 nM, which was lower than the estimated basal adenosine level *in vivo* (50~200 nM). And the limit of detection was 2 nM with S/N equals to 3. They applied this technique for *in vitro* measurement of adenosine in the PreBöttinger Complex (PreBötC) in the rat brain stem, a site rich in adenosine releasing neurons and is the commonly accepted site for respiratory rhythmogenesis. The diamond-based sensor was positioned into the PreBötC where only serotonin and adenosine are electrochemically active and can be distinguished by FSCV according to their different oxidation and reduction peak potentials. The *in vitro* adenosine detection from A_{2A} receptor activation results are shown in Figure 9. The data representing FSCV voltammograms obtained over time are compactly represented by the 3-D false color plot to map adenosine concentrations in the PreBötC of the rat brain. Although the exact release site of adenosine in the PreBötC was not located, the authors demonstrated the capability of a diamond-based probe for *in vitro* adenosine sensing in the central nervous system, and the possibility of investigating the role of adenosine in respiratory rhythmogenesis (i.e., the modulation of one's breathing rate) by using this sensor.

5.2.2. Serotonin (5-HT) measurement from aplysia californica metacerebral cell

Halpern *et al* recorded the serotonin level from the metacerebral cell in a marine mollusk, *Aplysia californica*, using a BDD microelectrode by FSCV (168). Specifically, the authors were trying to determine the release site and concentration of serotonin from the metacerebral cell, which has multiple roles in feeding behavior, such as biting, rejecting, and swallowing. Disk shaped diamond microelectrode with a diameter of 30 μ m was fabricated using the same method described above. A linear voltage sweep, from -0.4 to +1.2 V vs. Ag/AgCl, at a rate of 300 V/s was applied to detect the electrically stimulated release of serotonin, which had an oxidation peak at +0.958 V and a reduction peak at +0.362 V. This technique was then applied to the *in vitro* detection of serotonin at the I2 muscle fibers of the *Aplysia*. This study demonstrated the possibility of direct measurement of electrical activity from a specific cell. The capability of a BDD microelectrode working both as a sensor for electrical activity and a neural stimulating electrode was the key finding of this work. Diamond microelectrode arrays with these functions will possibly be applied for mapping the chemical and electrical signals *in vivo* during a complete feeding behavior in their future studies.

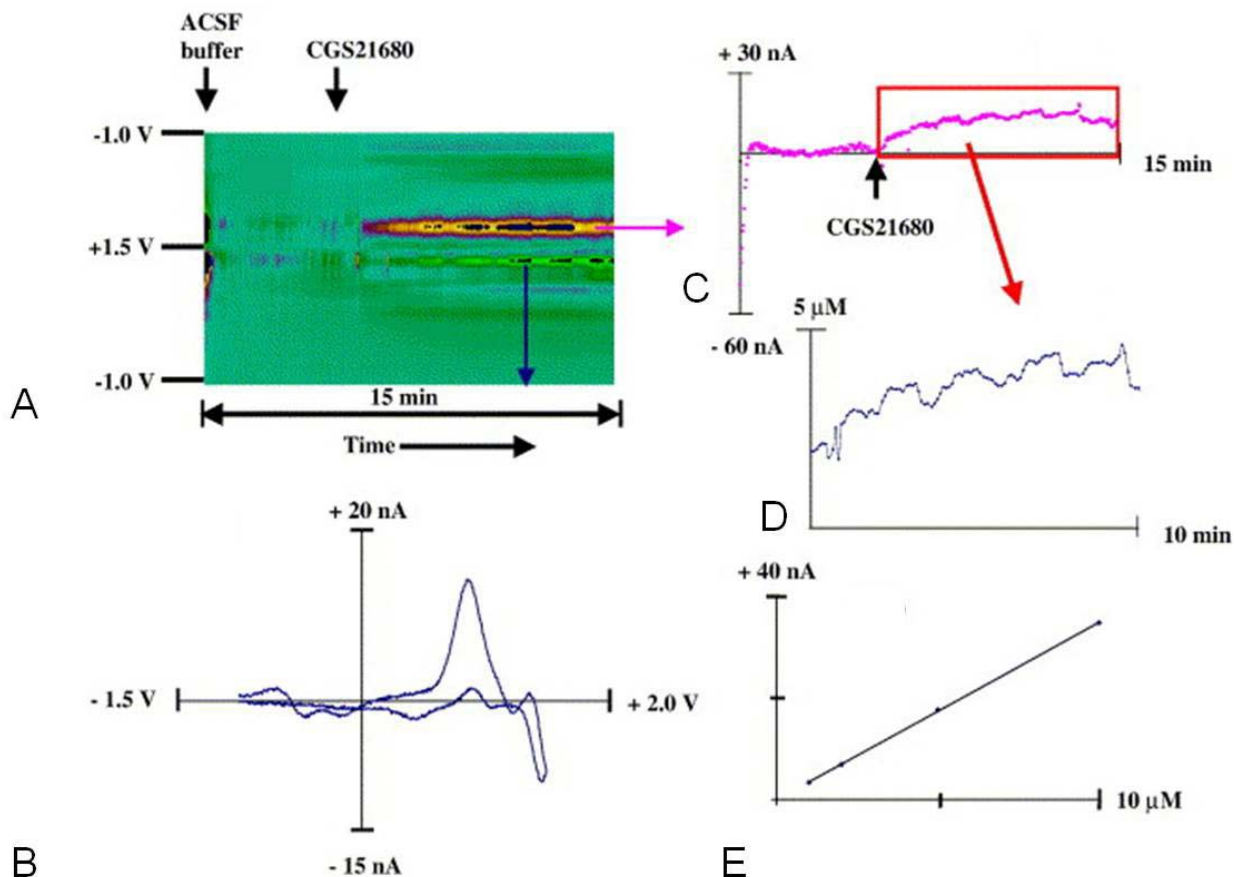


Figure 9. *In vitro* adenosine detection at a diamond microelectrode in the PreBötC region of a rat pup. (A), 3D false color plot shows the time varying voltammograms as adenosine is released upon CGS 21680 administration. (B), The cyclic voltammogram confirms adenosine release. (C), Adenosine oxidation current initially increased and then continually oscillated; the current data was converted to (D) the corresponding adenosine concentration by (E) post-calibration of the electrode with flow injection analysis. Reproduced with permission from ref (24).

6. CONCLUSIONS AND PERSPECTIVE

The studies presented in this review clearly demonstrate that BDD electrodes, without any polymer coating, can provide sensitive, stable and selective response for neurotransmitter detection *in vitro*. Due to its unique properties, such as small size, low background current and high resistance to fouling, BDD microelectrodes have shown a very promising future for biological research. Compared to other experimental approaches, e.g., microwave irradiation or microdialysis, electrochemical analysis with a BDD microelectrode can minimize serious tissue damage and provide high temporal resolution (24). However, there are also some challenges to overcome to advance the widespread use of BDD microelectrodes in physiological studies. First, methodology development for detection of biological molecules that are not electroactive can broaden the application of BDD microelectrodes. Some biological molecules also play very important roles as signaling molecules but cannot be detected by electrochemical methods because they are not electroactive, such as adenosine 5'-triphosphate (ATP). ATP is a

multifunctional nucleotide. Detection of ATP could be accomplished by coating the BDD with materials that could form an ATP sensor. For example, amperometric microbiosensors based on glucose oxidase and hexokinase immobilized within a polymer matrix at the surface of Pt disk microelectrodes were reported for the detection of extracellular ATP levels at rat carotid bodies (169). Utilization of proper polymer coatings may assist the use of BDD microelectrodes for the detection of non-electroactive compounds. Second, the size of the microelectrode needs to be reduced. One of the advantages of microelectrode is its high spatial resolution. The Holt and Fujishima groups have successfully fabricated BDD microelectrodes with diameter $< 5 \mu\text{m}$. However, this size is still considered large for single cell *in vitro* measurements. There has been report of the monitoring of real-time dopamine release from single living vesicles of single rat pheochromocytoma (PC12) cells by carbon fiber nanoelectrodes (tip diameter = *ca.* 100 nm) (170). In order to achieve the real time measurement of biological molecules from single vesicle, the size of the BDD microelectrode needs to be further reduced. The deposition of an evenly distributed ultra-thin

layer of BDD film onto the substrate is the most critical step for the minimization of microelectrodes, partially due to the existence of pinholes. An ordered BDD ultra-microelectrode array with optimum spacing could also be a future direction for the same analyte detection from different cells or several analytes detection from the same cell simultaneously (171, 172). Third, the reaction kinetics of various redox systems at diamond electrode surface is not well understood yet. Diamond electrodes have a sluggish response to catecholamines, such as norepinephrine, dopamine, and serotonin, but they do exhibit relatively fast electron transfer for some redox systems. *In vitro* electrochemical measurements of biomolecules are normally involved with the application of pharmacological agents. In the presence of some drugs, the microelectrode response to the molecules of interest may be altered by drug absorption onto the microelectrode surface (173). Therefore, the drug effects on electrode response sensitivity and stability should be determined before the *in vitro* electrochemical measurements of biomolecules with a BDD microelectrode.

7. REFERENCES

1. R. L. McCreery: Carbon electrodes: structural effects on electron transfer kinetics. *Electroanal Chem* 17, 221-374 (1990)
2. R. F. Davis: Diamond films and coatings: development, properties, and applications. Noyes, New Jersey (1993)
3. M. Iwaki, S. Sato, K. Takahashi and H. Sakairi: Electrical conductivity of nitrogen and argon implanted diamond. *Nucl Instrum Methods* 209/210, 1129-1133 (1983)
4. Y. V. Pelskov, A. Y. Sakharova, M. D. Krotova, L. L. Bouilov and B. V. Spitsyn: Photoelectrochemical properties of semiconductor diamond. *J Electroanal Chem* 228, 19-27 (1987)
5. J. S. Xu, M. C. Granger, Q. Y. Chen, J. W. Strojek, T. E. Lister and G. M. Swain: Boron-doped diamond thin-film electrodes. *Anal Chem* 69, A591-A597 (1997)
6. Q. Y. Chen and G. M. Swain: Structural characterization, electrochemical reactivity, and response stability of hydrogenated glassy carbon electrodes. *Langmuir* 14, 7017-7026 (1998)
7. R. Tenne and C. Levy-Clement: Diamond electrodes. *Isr J Chem* 38, 57-73 (1998)
8. A. Fujishima, Y. Einaga, T. N. Rao, D. A. Tryk and Editors: Diamond electrochemistry. BKC Tokyo Elsevier, Amsterdam (2005)
9. K. Peckova, J. Musilova and J. Barek: Boron-doped diamond film electrodes. New tool for voltammetric determination of organic substances. *Crit Rev Anal Chem* 39, 148-172 (2009)
10. G. M. Swain: Electrically conducting diamond thin films: advanced electrode materials for electrochemical technologies. *Electroanal Chem* 22, 181-277 (2004)
11. H. B. Martin, A. Argoitia, U. Landau, A. B. Anderson and J. C. Angus: Hydrogen and oxygen evolution on boron-doped diamond electrodes. *J Electrochem Soc* 143, L133-L136 (1996)
12. H. B. Martin, A. Argoitia, J. C. Angus and U. Landau: Voltammetry studies of single-crystal and polycrystalline diamond electrodes. *J Electrochem Soc* 146, 2959-2964 (1999)
13. M. C. Granger, M. Witek, J. Xu, J. Wang, M. Hupert, A. Hanks, M. D. Koppang, J. E. Butler, G. Lucazeau, M. Mermoux, J. W. Strojek and G. M. Swain: Standard electrochemical behavior of high-quality, boron-doped polycrystalline diamond thin-film electrodes. *Anal Chem* 72, 3793-3804 (2000)
14. A. E. Fischer, Y. Show and G. M. Swain: Electrochemical performance of diamond thin-film electrodes from different commercial sources. *Anal Chem* 76, 2553-2560 (2004)
15. Y. Maeda, K. Sato, R. Ramaraj, T. N. Rao, D. A. Tryk and A. Fujishima: The electrochemical response of highly boron-doped conductive diamond electrodes to Ce^{3+} ions in aqueous solution. *Electrochim Acta* 44, 3441-3449 (1999)
16. G. W. Muna, V. Quaiserova'-Mocko and G. M. Swain: Chlorinated phenol analysis using off-line solid-phase extraction and capillary electrophoresis coupled with amperometric detection and a boron-doped diamond microelectrode. *Anal Chem* 77, 6542-6548 (2005)
17. A. Fujishima, T. N. Rao, E. Popa, B. V. Sarada, I. Yagi and D. A. Tryk: Electroanalysis of dopamine and NADH at conductive diamond electrodes. *J Electrochem Soc* 473, 179-185 (1999)
18. M. Novotny, V. Quaiserov'a-Mocko, E. A. Wehrwein, D. L. Kreulen and G. M. Swain: Determination of endogenous norepinephrine levels in different chambers of the rat heart by capillary electrophoresis coupled with amperometric detection. *J Neurosci Methods* 163, 52-59 (2007)
19. B. V. Sarada, T. N. Rao, D. A. Tryk and A. Fujishima: Electrochemical oxidation of histamine and serotonin at highly boron doped diamond electrodes. *Anal Chem* 72, 1632-1638 (2000)
20. T. N. Rao, I. Yagi, T. Miwa, D. A. Tryk and A. Fujishima: Electrochemical oxidation of NADH at highly boron-doped diamond electrodes. *Anal Chem* 71, 2506-2511 (1999)
21. T. N. Rao, B. V. Sarada, D. A. Tryk and A. Fujishima: Electroanalytical study of sulfa drugs at diamond electrodes and their determination by HPLC with amperometric detection. *J Electroanal Chem* 491, 175-181 (2000)
22. J. B. Cooper, S. Pang, S. Albin, J. L. Zheng and R. M. Johnson: Fabrication of boron-doped CVD diamond microelectrodes. *Anal Chem* 70, 464-467 (1998)

Boron-doped diamond microelectrodes for *in vitro* measurements

23. J. Park, J. J. Galligan, G. D. Fink and G. M. Swain: *In vitro* continuous amperometry with a diamond microelectrode coupled with video microscopy for simultaneously monitoring endogenous norepinephrine and its effect on the contractile response of a rat mesenteric artery. *Anal Chem* 78, 6756-6764 (2006)
24. S. Xie, G. Shafer, C. G. Wilson and H. B. Martin: *In vitro* adenosine detection with a diamond-based sensor. *Diam Relat Mater* 15, 225 – 228 (2006)
25. B. A. Patel, X. Bian, V. Quaiserova'-Mocko, J. J. Galligan and G. M. Swain: *In vitro* continuous amperometric monitoring of 5-hydroxytryptamine release from enterochromaffin cells of the guinea pig ileum. *Analyst* 132, 41–47 (2007)
26. A. Suzuki, T. A. Ivandini, K. Yoshimi, A. Fujishima, G. Oyama, T. Nakazato, N. Hattori, S. Kitazawa and Y. Einaga: Fabrication, characterization, and application of boron-doped diamond microelectrodes for *in vivo* dopamine detection. *Anal Chem* 79, 8608-8615 (2007)
27. F. Gonon, J. X. Bao, M. Msghina, M. F. Saud-Chagny and L. Stjärne: Fast and local electrochemical monitoring of noradrenaline release from sympathetic terminals in isolated rat tail artery. *J Neurochem* 60, 1251-1257 (1993)
28. J. E. Baur, E. W. Kristensen, L. J. May, D. J. Wiedemann and R. M. Wightman: Fast-scan voltammetry of biogenic amines. *Anal Chem* 60, 1268-72 (1988)
29. J. A. Brock, W. R. Dunn, N. S. F. Boyd and D. K. Y. Wong: Spontaneous release of large packets of noradrenaline from sympathetic nerve terminals in rat mesenteric arteries *in vitro*. *Br J Pharmacol* 131, 1507 - 1511 (2000)
30. K. Tsunozaki, Y. Einaga, T. N. Rao and A. Fujishima: Fabrication and electrochemical characterization of boron-doped diamond microdisc array electrodes. *Chem Lett* 31, 502-503 (2002)
31. K. B. Holt, J. P. Hu and J. S. Foord: Fabrication of boron-doped diamond ultramicroelectrodes for use in scanning electrochemical microscopy experiments. *Anal Chem* 79, 2556-2561 (2007)
32. J. Cvacka, V. Quaiserova, J. Park, Y. Show, A. Muck and G. M. Swain: Boron-doped diamond microelectrodes for use in capillary electrophoresis with electrochemical detection. *Anal Chem* 75, 2678-2687 (2003)
33. J. Park, Y. Show, V. Quaiserova, J. J. Galligan, G. D. Fink and G. M. Swain: Diamond microelectrodes for use in biological environments. *J Electroanal Chem* 583, 56–68 (2005)
34. J. I. Friedman, D. N. Adler and K. L. Davis: The role of norepinephrine in the pathophysiology of cognitive disorders: Potential applications to the treatment of cognitive dysfunction in schizophrenia and Alzheimer's disease. *Biol Psychiatry* 46, 1243-1252 (1999)
35. M. Sarter and J. P. Bruno: Dopamine's role. *Science* 278, 1549-1550 (1997)
36. M. B. Hansen and A. B. Witte: The role of serotonin in intestinal luminal sensing and secretion. *Acta Physiol* 193, 311-323 (2008)
37. A. M. Sebastiao and J. A. Ribeiro: Adenosine receptors and the central nervous system. *Handb Exp Pharmacol* 193, 471-534 (2009)
38. L. Stjärne and E. Stjärne: Geometry, kinetics and plasticity of release and clearance of ATP and noradrenaline as sympathetic cotransmitters: roles for the neurogenic contraction. *Prog Neurobiol* 47, 45-94 (1995)
39. J. E. Field: The properties of natural and synthetic diamond. Academic Press (1992)
40. M. I. Landstrass and K. V. Ravi: Resistivity of chemical vapor-deposited diamond films. *Appl Phys Lett* 55, 975-977 (1989)
41. S. C. Eaton, A. B. Anderson, J. C. Angus, Y. E. Evstefeeva and Y. V. Pleskov: Co-doping of diamond with boron and sulfur. *Electrochem Solid St Lett* 5, G65-G68 (2002)
42. S. Miyajima, M. Kim, Y. Ide, A. Yamada and M. Konagai: Highly conductive boron doped microcrystalline Si films deposited by hot wire cell method and its application to solar cells. *Jpn J Appl Phys* 42, 3328-3332 (2003)
43. J. Birrell, J. A. Carlisle, O. Auciello, D. M. Gruen and J. M. Gibson: Morphology and electronic structure in nitrogen-doped ultrananocrystalline diamond. *Appl Phys Lett* 81, 2235-2237 (2002)
44. S. Koizumi, M. Kamo, Y. Sato, H. Ozaki and T. Inuzuka: Growth and characterization of phosphorus doped {111} homoepitaxial diamond thin films. *Appl Phys Lett* 71, 1065-1067 (1997)
45. K. Okano, H. Kiyota, T. Iwasaki, Y. Nakamura, Y. Akiba, T. Kurosu, M. Iida and T. Nakamura: Synthesis of N-type semiconducting diamond film using diphosphorus pentoxide as the doping source. *Appl Phys A* 51, 344-346 (1990)
46. A. E. Aleksenko and B. V. Spitsyn: Semiconducting diamonds made in the USSR. *Diam Relat Mater* 1, 705-9 (1992)
47. J. C. Angus, H. A. Will and W. S. Stanko: Growth of diamond seed crystals by vapor deposition. *J Appl Phys* 39, 2915-2922 (1968)
48. B. V. Derjaguin, D. V. Fedoseev, V. M. Lukyanovich, B. V. Spitzin, V. A. Ryabov and A. V. Lavrentyev: Filamentary diamond crystals *J Cryst Growth* 2, 380-384 (1968)

Boron-doped diamond microelectrodes for *in vitro* measurements

49. J. Asmussen and D. K. Reinhard: Diamond films handbook. Marcel Dekker, New York (2002)
50. M. Frenklach and K. E. Spear: Growth-mechanism of vapor-deposited diamond. *J Mater Res* 3, 133-140 (1988)
51. J. C. Angus and C. C. Hayman: Low-pressure, metastable growth of diamond and "diamondlike" phases. *Science* 241, 913-921 (1988)
52. P. E. Pehrsson, F. G. Celii and J. E. Butler: Chemical mechanisms of diamond CVD. In : Diamond films and coatings: development, properties, and applications. Set 3. Eds: R.F. Foster, Noyes, New Jersey (1993)
53. J. E. Butler and R. L. Woodin: Thin-film diamond growth mechanisms. *Phil Trans R Soc Lond* 342, 209-224 (1993)
54. M. Fryda, T. Matthee, S. Mulcahy, A. Hampel, L. Schafer and I. Troster: Fabrication and application of Diachem (R) electrodes. *Diam Relat Mater* 12, 1950-1956 (2003)
55. A. V. Sumant, P. U. P. A. Gilbert, D. S. Grierson, A. R. Konicek, M. Abrecht, J. E. Butler, T. Feygelson, S. S. Rotter and R. W. Carpick: Surface composition, bonding, and morphology in the nucleation and growth of ultra-thin, high quality nanocrystalline diamond films. *Diam Relat Mater* 16, 718-724 (2007)
56. J. E. Butler and A. V. Sumant: The CVD of nanodiamond materials. *Chem Vap Deposition* 14, 145-160 (2008)
57. J. Philip, P. Hess, T. Feygelson, J. E. Butler, S. Chattopadhyay, K. H. Chen and L. C. Chen: Elastic, mechanical, and thermal properties of nanocrystalline diamond films. *J Appl Phys* 93, 2164-2171 (2003)
58. Y. Show, M. A. Witek, P. Sonthalia and G. M. Swain: Characterization and electrochemical responsiveness of boron-doped nanocrystalline diamond thin-film electrodes. *Chem Mater* 15, 879-888 (2003)
59. D. M. Gruen: Nanocrystalline diamond films. *Annu Rev Mater Sci* 29, 211-259 (1999)
60. D. Zhou, T. G. McCauley, L. C. Qin, A. R. Krauss and D. M. Gruen: Synthesis of nanocrystalline diamond thin films from an Ar-CH₄ microwave plasma. *J Appl Phys* 83, 540-543 (1998)
61. J. Birrell, J. E. Gerbi, O. Auciello, J. M. Gibson, D. M. Gruen and J. A. Carlisle: Bonding structure in nitrogen doped ultrananocrystalline diamond. *J Appl Phys* 93, 5606-5612 (2003)
62. D. M. Gruen: Nucleation, growth, and microstructure of nanocrystalline diamond films. *MRS Bull* 23, 32-35 (1998)
63. P. Zapol, M. Sternberg, L. A. Curtiss, T. Frauenheim and D. M. Gruen: Tight-binding molecular-dynamics simulation of impurities in ultrananocrystalline diamond grain boundaries. *Phys Rev B* 65, 045403/1-045403/11 (2002)
64. M. Sternberg, P. Zapol and L. A. Curtiss: Carbon dimers on the diamond (100) surface: Growth and nucleation. *Phys Rev B* 68, 205330/1- 205330/9 (2003)
65. S. Wang, V. M. Swope, J. E. Bulter, T. Feygelson and G. M. Swain: The structural and electrochemical properties of boron-doped nanocrystalline diamond thin-film electrodes grown from Ar-rich and H₂-rich source gases. *Diam Relat Mater* 18, 669-677 (2009)
66. J. Park, V. Quaiserova'-Mocko, K. Peckova, J. J. Galligan, G. D. Fink and G. M. Swain: Fabrication, characterization, and application of a diamond microelectrode for electrochemical measurement of norepinephrine release from the sympathetic nervous system. *Diam Relat Mater* 15, 761-772 (2006)
67. D. C. Shin, B. V. Sarada, D. A. Tryk and A. Fujishima: Application of diamond microelectrodes for end-column electrochemical detection in capillary electrophoresis. *Anal Chem* 75, 530-534 (2003)
68. B. V. Sarada, T. N. Rao, D. A. Tryk and A. Fujishima: Electrochemical characterization of highly boron-doped diamond microelectrodes in aqueous electrolyte. *J Electrochem Soc* 146, 1469-1471 (1999)
69. H. Olivia, B. V. Sarada, D. Shin, T. N. Rao and A. Fujishima: Selective amperometric detection of dopamine using OPPy-modified diamond microsensor system. *Analyst* 127, 1572-1575 (2002)
70. S. Basu, W. P. Kang, J. L. Davidson, B. K. Choi, A. B. Bonds and D. E. Cliffel: Electrochemical sensing using nanodiamond microprobe. *Diam Relat Mater* 15, 269-274 (2006)
71. K. B. Holt, D. J. Caruana, J. Raja, J. Hu and J. S. Foord: Fabrication and characterization of diamond ultramicroelectrodes of diameter < 25 micron for use in electroanalysis, sensing and imaging applications *ECS Trans* 3, 37-45 (2007)
72. G. W. Muna, N. Tasheva and G. M. Swain: Electro-oxidation and amperometric detection of chlorinated phenols at boron-doped diamond electrodes: A comparison of microcrystalline and nanocrystalline thin films. *Environ Sci Technol* 38, 3674-3682 (2004)
73. Z. Zhou and S. Mislser: Amperometric detection of quantal secretion from patch-clamped rat pancreatic beta-cells. *J Biol Chem* 271, 270-277 (1996)
74. R. H. Chow, L. Vonruden and E. Neher: Delay in vesicle fusion revealed by electrochemical monitoring of single secretory events in adrenal chromaffin cells. *Nature* 356, 60-63 (1992)

75. O. A. Williams, M. Nesladek, M. Daenen, S. Michaelson, A. Hoffman, E. Osawa, K. Haenen and R. B. Jackman: Growth, electronic properties and applications of nanodiamond. *Diam Relat Mater* 17, 1080-1088 (2008)
76. E. Mahe, D. Devilliers and C. Comminellis: Electrochemical reactivity at graphitic micro-domains on polycrystalline boron doped diamond thin-films electrodes. *Electrochim Acta* 50, 2263-2277 (2005)
77. O. Enea, B. Riedo and G. Dietler: AFM study of Pt clusters electrochemically deposited onto boron-doped diamond films. *Nano Lett* 2, 241-244 (2002)
78. K. B. Holt, A. J. Bard, Y. Show and G. M. Swain: Scanning electrochemical microscopy and conductive probe atomic force microscopy studies of hydrogen-terminated boron-doped diamond electrodes with different doping levels. *J Phys Chem B* 108, 15117-15127 (2004)
79. N. R. Wilson, S. L. Clewes, M. E. Newton, P. R. Unwin and J. V. Macpherson: Impact of grain-dependent boron uptake on the electrochemical and electrical properties of polycrystalline boron doped diamond electrodes. *J Phys Chem B* 110, 5639-5646 (2006)
80. S. Wang and G. M. Swain: Spatially heterogeneous electrical and electrochemical properties of hydrogen-terminated boron-doped nanocrystalline diamond thin film deposited from an argon-rich CH₄/H₂/Ar/B₂H₆ source gas mixture. *J Phys Chem C* 111, 3986-3995 (2007)
81. J. R. Dennison, M. Holtz and G. Swain: Raman spectroscopy of carbon materials. *Spectroscopy* 11, 38-46 (1996)
82. M. Mermoux, B. Marcus, G. M. Swain and J. E. Butler: A confocal Raman imaging study of an optically transparent boron-doped diamond electrode. *J Phys Chem B* 106, 10816-10827 (2002)
83. S. Praver, K. W. Nugent, D. N. Jamieson, J. O. Orwa, L. A. Bursill and J. L. Peng: The Raman spectrum of nanocrystalline diamond. *Chem Phys Lett* 332, 93-97 (2000)
84. Y. Wang, D. C. Alsmeyer and R. L. McCreery: Raman-spectroscopy of carbon materials - structural basis of observed spectra. *Chem Mater* 2, 557-563 (1990)
85. W. A. Yarbrough and R. Messier: Current issues and problems in the chemical vapor-deposition of diamond. *Science* 247, 688-696 (1990)
86. Z. L. Wang, C. Lu, J. J. Li and C. Z. Gu: Effect of gas composition on the growth and electrical properties of boron-doped diamond films. *Diam Relat Mater* 18, 132-135 (2009)
87. J. B. Zang, Y. H. Wang, H. Huang and W. Q. Liu: Electrochemical characteristics of boron doped polycrystalline diamond electrode sintered by high pressure and high temperature. *J Appl Electrochem* 39, 1545-1551 (2009)
88. J. C. Zhang, J. W. Zimmer, R. T. Howe and R. Maboudian: Characterization of boron-doped micro- and nanocrystalline diamond films deposited by wafer-scale hot filament chemical vapor deposition for MEMS applications. *Diam Relat Mater* 17, 23-28 (2008)
89. T. Kondo, H. Ito, K. Kusakabe, K. Ohkawa, Y. Einaga, A. Fujishima and T. Kawai: Plasma etching treatment for surface modification of boron-doped diamond electrodes. *Electrochim Acta* 52, 3841-3848 (2007)
90. G. Shul, P. Actis, B. Marcus, M. Opallo, R. Boukherroub and S. Szunerits: Solvent-free chemical functionalization of hydrogen-terminated boron-doped diamond electrodes with diazonium salts in ionic liquids. *Diam Relat Mater* 17, 1394-1398 (2008)
91. S. Gupta, M. Muralikiran, J. Farmer, L. R. Cao and R. G. Downing: The effect of boron doping and gamma irradiation on the structure and properties of microwave chemical vapor deposited boron-doped diamond films. *J Mater Res* 24, 1498-1512 (2009)
92. I. B. Altfeder, J. J. Hu, A. A. Voevodin and J. Krim: Magic-sized diamond nanocrystals. *Phys Rev Lett* 102, 136104/1-136104/4 (2009)
93. M. Murakami, T. Shimizu, M. Tansho, Y. Takano, S. Ishii, E. A. Ekimov, V. A. Sidorov, H. Sumiya, H. Kawarada and K. Takegoshi: Characterization of boron-doped diamonds using B-11 high-resolution NMR at high magnetic fields. *Diam Relat Mater* 17, 1835-1839 (2008)
94. S. H. Baek, N. J. Curro, E. A. Ekimov, V. A. Sidorov, E. D. Bauer and J. D. Thompson: Impurity band in B-doped diamond: an B-11 NMR study. *Supercond Sci Tech* 22, 065008/1-065008/5 (2009)
95. N. Habka, M. A. Pinault, C. Mer, F. Jomard, J. Barjon, M. Nesladek and P. Bergonzo: Substrate influence on MPCVD boron-doped homoepitaxial diamond. *Physica Status Solidi A: Appl Mater Sci* 205, 2169-2172 (2008)
96. S. Ghodbane, F. Omnes and C. Agnes: A cathodoluminescence study of boron doped {111}-homoepitaxial diamond films. *Diam Relat Mater* 19, 273-278 (2010)
97. V. Mortet, M. Daenen, T. Teraji, A. Lazea, V. Vorlicek, J. D'Haen, K. Haenen and M. D'Olienslaeger: Characterization of boron doped diamond epilayers grown in a NIRIM type reactor. *Diam Relat Mater* 17, 1330-1334 (2008)
98. N. Tsubouchi and M. Ogura: Enhancement of dopant activation in B-implanted diamond by high-temperature annealing. *Jap J Appl Phys* 47, 7047-7051 (2008)
99. S. M. Hearne, E. Trajkov, D. N. Jamieson, J. E. Butler and S. Praver: The role of charge trapping at grain boundaries on charge transport in polycrystalline chemical vapor deposited diamond based detectors. *J Appl Phys* 99, 113703/1-113703/8 (2006)

Boron-doped diamond microelectrodes for *in vitro* measurements

100. Y. G. Wang, H. D. Li, Y. Y. Xiong, S. L. Zhang, Z. D. Lin and K. Feng: Micro-Raman scattering and photoluminescence study of boron-doped diamond films. *Diam Relat Mater* 9, 1708-1711 (2000)
101. K. R. Kneten and R. L. McCreery: Effects of redox system structure on electron-transfer kinetics at ordered graphite and glassy-carbon electrodes. *Anal Chem* 64, 2518-2524 (1992)
102. P. Chen, M. A. Fryling and R. L. McCreery: Electron transfer kinetics at modified carbon electrode surfaces: the role of specific surface sites. *Anal Chem* 67, 3115-3122 (1995)
103. P. H. Chen and R. L. McCreery: Control of electron transfer kinetics at glassy carbon electrodes by specific surface modification. *Anal Chem* 68, 3958-3965 (1996)
104. M. J. Loiacono, E. L. Granstrom and C. D. Frisbie: Investigation of charge transport in thin, doped sexithiophene crystals by conducting probe atomic force microscopy. *J Phys Chem B* 102, 1679-1688 (1998)
105. T. W. Kelley, E. L. Granstrom and C. D. Frisbie: Conducting probe atomic force microscopy: A characterization tool for molecular electronics. *Adv Mater* 11, 261-264 (1999)
106. J. V. Macpherson, J. P. G. de Mussy and J. L. Delplanck: Conducting-atomic force microscopy investigation of the local electrical characteristics of a Ti/TiO₂/Pt anode. *Electrochem Solid St Lett* 4, E33-E36 (2001)
107. O. Ternyak, A. A. Cimmino, S. Praver and A. Hoffman: Ultrathin continuous undoped diamond films: Investigation of nanoscale conduction properties. *Diam Relat Mater* 14, 272-278 (2005)
108. M. C. Granger, J. S. Xu, J. W. Strojek and G. M. Swain: Polycrystalline diamond electrodes: basic properties and applications as amperometric detectors in flow injection analysis and liquid chromatography. *Anal Chim Acta* 397, 145-161 (1999)
109. K. Ushizawa, K. Watanabe, T. Ando, I. Sakaguchi, M. Nishitani-Gamo, Y. Sato and H. Kanda: Boron concentration dependence of Raman spectra on {100} and {111} facets of B-doped CVD diamond. *Diam Relat Mater* 7, 1719-1722 (1998)
110. S. J. Charles, J. W. Steeds, D. J. F. Evans, S. Lawson and J. E. Butler: Characterisation of electron irradiated boron-doped diamond. *Diam Relat Mater* 11, 681-685 (2002)
111. A. C. Ferrari and J. Robertson: Origin of the 1150-cm(-1) raman mode in nanocrystalline diamond. *Phys Rev B* 63, 121405/1-121405/4 (2001)
112. J. Birrell, J. E. Gerbi, O. Auciello, J. M. Gibson, J. Johnson and J. A. Carlisle: Interpretation of the Raman spectra of ultrananocrystalline diamond. *Diam Relat Mater* 14, 86-92 (2005)
113. J. W. Ager, W. Walukiewicz, M. McCluskey, M. A. Plano and M. I. Landstrass: Fano interference of the raman phonon in heavily boron-doped diamond films grown by chemical-vapor-deposition. *Appl Phys Lett* 66, 616-618 (1995)
114. P. Gonon, A. Deneuve, F. Fontaine and E. Gheeraert: Electrical-conduction and deep levels in polycrystalline diamond films. *J Appl Phys* 78, 6633-6638 (1995)
115. I. F. Hu, D. H. Karweik and T. Kuwana: Activation and deactivation of glassy-carbon electrodes. *J Electroanal Chem* 188, 59-72 (1985)
116. T.-C. Kuo and R. L. McCreery: Surface chemistry and electron-transfer kinetics of hydrogen-modified glassy carbon electrodes. *Anal Chem* 71, 1553-1560 (1999)
117. J. Wang, G. M. Swain, M. Mermoux, G. Lucazeau, J. Zak and J. W. Strojek: Probing the microstructure and electrochemical reactivity of boron-doped diamond thin-film electrodes with Raman microprobe spectroscopy and electrogenerated chemiluminescence imaging analysis. *New Diamond Front Carbon Technol* 9, 317-343 (1999)
118. M. R. Deakin, K. J. Stutts and R. M. Wightman: The effect of Ph on some outer-sphere electrode-reactions at carbon electrodes. *J Electroanal Chem* 182, 113-122 (1985)
119. L. M. Peter, W. Durr, P. Bindra and H. Gerischer: Influence of alkali-metal cations on rate of Fe(Cn)⁴⁺(6)/Fe(Cn)³⁺(6) electrode process. *J Electroanal Chem* 71, 31-50 (1976)
120. M. Noel and P. N. Anantharaman: Voltammetric studies on a glassy-carbon electrode. 2. factors influencing the simple electron-transfer reactions - the K₃[Fe(Cn)⁶⁺]-K₄[Fe(Cn)⁶⁺] system. *Analyst* 110, 1095-1103 (1985)
121. M. C. Granger and G. M. Swain: The influence of surface interactions on the reversibility of ferri/ferrocyanide at boron-doped diamond thin-film electrodes. *J Electrochem Soc* 146, 4551-4558 (1999)
122. J. Wang and G. M. Swain: Fabrication and evaluation of platinum/diamond composite electrodes for electrocatalysis - Preliminary studies of the oxygen-reduction reaction. *J Electrochem Soc* 150, E24-E32 (2003)
123. G. M. Swain, A. B. Anderson and J. C. Angus: Applications of diamond thin films in electrochemistry. *MRS Bull* 23, 56-60 (1998)
124. N. Vinokur, B. Miller, Y. Avyigal and R. Kalish: Electrochemical behavior of boron-doped diamond electrodes. *J Electrochem Soc* 143, L238-L240 (1996)
125. S. Ranganathan, T.-C. Kuo and R. L. McCreery: Facile preparation of active glassy carbon electrodes with

Boron-doped diamond microelectrodes for *in vitro* measurements

- activated carbon and organic solvents. *Anal Chem* 71, 3574–3580 (1999)
126. S. Alehashem, F. Chambers, J. W. Strojek, G. M. Swain and R. Ramesham: Cyclic voltammetric studies of charge-transfer reactions at highly boron-doped polycrystalline diamond thin-film electrodes. *Anal Chem* 67, 2812-2821 (1995)
127. H. H. Yang and R. L. McCreery: Effects of surface monolayers on the electron-transfer kinetics and adsorption of methyl viologen and phenothiazine derivatives on glassy carbon electrodes. *Anal Chem* 71, 4081-4087 (1999)
128. K. K. Cline, M. T. Mcdermott and R. L. McCreery: Anomalous slow-electron transfer at ordered graphite-electrodes - influence of electronic factors and reactive sites. *J Phys Chem* 98, 5314-5319 (1994)
129. A. J. Bard and L. R. Faulkner: Electrochemical methods fundamentals and applications. John Wiley and Sons Inc., New York (2001)
130. C. G. Zoski and M. V. Mirkin: Steady-state limiting currents at finite conical microelectrodes. *Anal Chem* 74, 1986-1992 (2002)
131. G. M. Swain and R. Ramesham: The electrochemical activity of boron-doped polycrystalline diamond thin film electrodes. *Anal Chem* 65, 345-351 (1993)
132. D. Leszczyszyn, J. Jankowski, O. Viveros, E. J. Diliberto, J. Near and R. Wightman: Secretion of catecholamines from individual adrenal medullary chromaffin cells. *J Neurochem* 56, 1855-63 (1991)
133. J. A. Brock and J. H. C. Tan: Selective modulation of noradrenaline release by α_2 -adrenoceptor blockade in the rat-tail artery *in vitro*. *Br J Pharmacol* 142, 267–274 (2004)
134. E. R. Travis and R. M. Wightman: Spatio-temporal resolution of exocytosis from individual cells. *Annu Rev Biophys Biomol Struct* 27, 77-103 (1998)
135. D. Bruns and R. Jahn: Real-time measurement of transmitter release from single synaptic vesicles. *Nature* 377, 62-5 (1995)
136. J. G. Hardman, L. E. Limbird and A. G. Gilman: The pharmacological basis of therapeutics. McGraw-Hill Professional, (2001)
137. F. Gonon, M. Msghina and L. Stjarne: Kinetics of noradrenaline released by sympathetic nerves. *Neuroscience* 56, 535-538 (1993)
138. W. R. Dunn, T. A. Hardy and J. A. Brock: Electrophysiological effects of activating the peptidergic primary afferent innervation of rat mesenteric arteries. *Br J Pharmacol* 140, 231–238 (2003)
139. J. A. Stamford, P. Palij, C. Davidson, C. M. Jorm and J. Millarb: Simultaneous “real-time” electrochemical and electrophysiological recording in brain slices with a single carbon-fibre microelectrode. *J Neurosci Methods* 50, 279-290 (1993)
140. G. M. Mawe, M. D. Coates and P. L. Moses: Review article: intestinal serotonin signalling in irritable bowel syndrome. *Aliment Pharmacol Ther* 23, 1067-1076 (2006)
141. G. Dryhurst: Applications of electrochemistry in studies of the oxidation chemistry of central-nervous-system Indoles. *Chem Rev* 90, 795-811 (1990)
142. M. Z. Wrona and G. Dryhurst: Oxidation chemistry of 5-Hydroxytryptamine. *J Electrochem Soc* 134, C135-C135 (1987)
143. P. P. Bertrand: Real-time detection of serotonin release from enterochromaffin cells of the guinea-pig ileum. *Neurogastroenterol Motil* 16, 511-514 (2004)
144. B. P. Jackson, S. M. Dietz and R. M. Wightman: Fast-scan cyclic voltammetry of 5-hydroxytryptamine. *Anal Chem* 67, 1115-1120 (1995)
145. H. Zhao, X. C. Bian, J. J. Galligan and G. M. Swain: Electrochemical measurements of serotonin (5-HT) release from the guinea pig mucosa using continuous amperometry with a boron-doped diamond microelectrode. *Diam Relat Mater* 19, 182-185 (2010)
146. B. A. Patel, X. Dai, J. E. Burda, H. Zhao, G. M. Swain, J. J. Galligan and X. Bian: Inhibitory neuromuscular transmission to ileal longitudinal muscle predominates in neonatal guinea pigs. *Neurogastroenterol Motil* 22, 909-E237 (2010)
147. D. P. Manica, Y. Mitsumori and A. G. Ewing: Characterization of electrode fouling and surface regeneration for a platinum electrode on an electrophoresis microchip. *Anal Chem* 75, 4572-4577 (2003)
148. X. C. Bian, B. Patel, X. L. Dai, J. J. Galligan and G. M. Swain: High mucosal serotonin availability in neonatal guinea pig ileum is associated with low serotonin transporter expression. *Gastroenterology* 132, 2438-2447 (2007)
149. B. A. Patel: Continuous amperometric detection of co-released serotonin and melatonin from the mucosa in the ileum. *Analyst* 133, 516-524 (2008)
150. N. T. Raikhlin, I. M. Kvetnoy and V. N. Tolkachev: Melatonin may be synthesized in enterochromaffin cells. *Nature* 255, 344-345 (1975)
151. Y. S. Singh, L. E. Sawarynski, H. M. Michael, R. E. Ferrell, M. A. Murphey-Corb, G. M. Swain, B. A. Patel and A. M. Andrews: Boron-doped diamond microelectrodes reveal reduced serotonin uptake rates in lymphocytes from adult rhesus monkeys carrying the short

Boron-doped diamond microelectrodes for *in vitro* measurements

- allele of the 5-HTTLPR. *ACS Chem Neurosci* 1, 49-64 (2010)
152. T. Takahashi: Pathophysiological significance of neuronal nitric oxide synthase in the gastrointestinal tract. *J Gastroenterol* 38, 421-430 (2003)
153. H. Iwasaki, M. Kajimura, S. Osawa, S. Kanaoka, T. Furuta, M. Ikuma and A. Hishida: A deficiency of gastric interstitial cells of Cajal accompanied by decreased expression of neuronal nitric oxide synthase and substance P in patients with type 2 diabetes mellitus. *J Gastroenterol* 41, 1076-1087 (2006)
154. C. Amatore, S. Arbault, Y. Bouret, B. Cauli, M. Guille, A. Rancillac and J. Rossier: Nitric oxide release during evoked neuronal activity in cerebellum slices: Detection with platinumized carbon-fiber microelectrodes. *Chemphyschem* 7, 181-187 (2006)
155. B. A. Patel, M. Arundell, K. H. Parker, M. S. Yeoman and D. O'Hare: Detection of nitric oxide release from single neurons in the pond snail, *Lymnaea stagnalis*. *Anal Chem* 78, 7643-7648 (2006)
156. N. R. Ferreira, A. Ledo, J. G. Frade, G. A. Gerhardt, J. Laranjinha and R. M. Barbosa: Electrochemical measurement of endogenously produced nitric oxide in brain slices using Nafion/o-phenylenediamine modified carbon fiber microelectrodes. *Anal Chim Acta* 535, 1-7 (2005)
157. B. A. Patel, J. J. Galligan, G. M. Swain and X. Bian: Electrochemical monitoring of nitric oxide released by myenteric neurons of the guinea pig ileum. *Neurogastroenterol Motil* 20, 1243-1250 (2008)
158. S. Kamoshida, E. Saito, S. Fukuda, K. Kato, A. Iwasaki and Y. Arakawa: Anatomical location of enterochromaffin-like (ECL) cells, parietal cells, and chief cells in the stomach demonstrated by immunocytochemistry and electron microscopy. *J Gastroenterol* 34, 315-320 (1999)
159. V. Fykse, E. Solligard, M. O. Bendheim, D. Chen, J. E. Gronbech, A. K. Sandvik and H. L. Waldum: ECL cell histamine mobilization and parietal cell stimulation in the rat stomach studied by microdialysis and electron microscopy. *Acta Physiol* 186, 37-43 (2006)
160. R. Hakanson, D. Chen, E. Lindstrom, M. Bernsand and P. Norlen: Control of secretion from rat stomach ECL cells *in situ* and in primary culture. *Scand J Clin Lab Invest* 61, 53-60 (2001)
161. H. L. Waldum, A. K. Sandvik, E. Brenna and H. Petersen: Gastrin-histamine sequence in the regulation of gastric-acid secretion. *Gut* 32, 698-701 (1991)
162. E. Bitziou, D. O'Hare and B. A. Patel: Simultaneous detection of pH changes and histamine release from oxyntic glands in isolated stomach. *Anal Chem* 80, 8733-8740 (2008)
163. K. T. Kawagoe, J. B. Zimmerman and R. M. Wightman: Principles of voltammetry and microelectrode surface states. *J Neurosci Methods* 48, 225-240 (1993)
164. K. P. Troyer, M. L. Heien, B. J. Venton and R. M. Wightman: Neurochemistry and electroanalytical probes. *Curr Opin Chem Biol* 6, 696-703 (2002)
165. J. Stamford: *In vivo* voltammetry: some methodological considerations. *J Neurosci Methods* 17, 1-29 (1986)
166. R. M. Wightman: Voltammetry with microscopic electrodes in new domains. *Science* 24, 415 - 420 (1988)
167. E. Popa, H. Notsu, T. Miwa, D. A. Tryk and A. Fujishima: Selective electrochemical detection of dopamine in the presence of ascorbic acid at anodized diamond thin film electrodes. *Electrochem Solid State Lett* 2, 49-51 (1999)
168. J. M. Halpern, S. T. Xie, G. P. Sutton, B. T. Higashikubo, C. A. Chestek, H. Lu, H. J. Chiel and H. B. Martin: Diamond electrodes for neurodynamic studies in *Aplysia californica*. *Diam Relat Mater* 15, 183-187 (2006)
169. J. F. Masson, C. Kranz, B. Mizaikoff and E. B. Gauda: Amperometric ATP microbiosensors for the analysis of chemosensitivity at rat carotid bodies. *Anal Chem* 80, 3991-3998 (2008)
170. W. Z. Wu, W. H. Huang, W. Wang, Z. L. Wang, J. K. Cheng, R. Y. Zhang, Y. Chen, J. Liu, C. Y. Zheng and C. Shen: Nanoelectrode-patch clamp monitoring of continual single living vesicle release. *Chem J Chinese U* 26, 829-831 (2005)
171. A. Bonnauron, S. Saada, L. Rousseau, G. Lissorgues, C. Mer and P. Bergonzo: High aspect ratio diamond microelectrode array for neuronal activity measurements. *Diam Relat Mater* 17, 1399-1404 (2008)
172. S. Raina, W. P. Kang and J. L. Davidson: Fabrication of nitrogen-incorporated nanodiamond ultra-microelectrode array for dopamine detection. *Diam Relat Mater* 19, 256-259 (2010)
173. H. Dong, S. Wang, A. Liu, J. J. Galligan and G. M. Swain: Drug effects on the electrochemical detection of norepinephrine with carbon fiber and diamond microelectrodes. *J Electroanal Chem* 632, 20-29 (2009)

Abbreviations: BDD: boron-doped diamond; CVD: chemical vapor deposition; NCD: nanocrystalline diamond; UNCD: ultra nanocrystalline diamond; MPCVD: microwave plasma-assisted chemical vapor deposition; SEM: scanning electron microscopy; AFM: atomic force microscopy; CP-AFM: conductive probe AFM; XRD: X-ray diffraction; XPS: X-ray photoelectron spectroscopy; FSCV: fast scan cyclic voltammetry; NE: norepinephrine; 5-HT: 5-hydroxytryptamine; NO: nitric

Boron-doped diamond microelectrodes for *in vitro* measurements

oxide; NADH: nicotinamide adenine dinucleotide; EC: enterochromaffin; SERT: serotonin transporter; ECL: enterochromaffin-like; PreBötC: PreBötzing Complex; ATP: adenosine 5'-triphosphate

Key Words: Boron-doped diamond nano/microelectrode, *In vitro* measurement, Amperometry, Fast scan cyclic voltammetry, Norepinephrine, Serotonin, Nitric Oxide, Histamine, Adenosine, Review

Send correspondence to: Hua Dong, Department of Entomology and Cancer Research Center, University of California, Davis, CA, 95616, Tel: 530-752-5109, Fax: 530-752-1537, E-mail: hdong@ucdavis.edu

<http://www.bioscience.org/current/vol3S.htm>